Published in final edited form as:

Cell Rep. 2023 December 26; 42(12): 113471. doi:10.1016/j.celrep.2023.113471.

Co-transmitting interneurons in the mouse olfactory bulb regulate olfactory detection and discrimination

Ariel M. Lyons-Warren[1], **Evelyne K. Tantry**[2], **Elizabeth H. Moss**[2], **Mikhail Y. Kochukov**[2], **Benjamin D.W. Belfort**[2,3], **Joshua Ortiz-Guzman**[2], **Zachary Freyberg**[4,5], **Benjamin R. Arenkiel**[2,6,*]

[1]Department of Pediatrics, Section of Pediatric Neurology and Developmental Neuroscience, Baylor College of Medicine, Jan and Dan Duncan Neurological Research Institute, Texas Children's Hospital, 1250 Moursund Street, Houston, TX 77030, USA

[2]Department of Molecular and Human Genetics, Baylor College of Medicine, Jan and Dan Duncan Neurological Research Institute, Texas Children's Hospital, 1250 Moursund Street, Houston, TX 77030, USA

[3]Medical Scientist Training Program, Baylor College of Medicine, 1 Baylor Plaza, Houston, TX 77030, USA

[4]Department of Psychiatry, University of Pittsburgh, Pittsburgh, PA 15213, USA

[5]Department of Cell Biology, University of Pittsburgh, Pittsburgh, PA 15213, USA

[6]Lead contact

SUMMARY

Co-transmission of multiple neurotransmitters from a single neuron increases the complexity of signaling information within defined neuronal circuits. Superficial short-axon cells in the olfactory bulb release both dopamine and γ-aminobutyric acid (GABA), yet the specific targets of these neurotransmitters and their respective roles in olfaction have remained unknown. Here, we implement intersectional genetics in mice to selectively block GABA or dopamine release from superficial short-axon cells to identify their distinct cellular targets, impact on circuit function, and behavioral contribution of each neurotransmitter toward olfactory behaviors. We provide functional and anatomical evidence for divergent superficial short-axon cell signaling onto downstream neurons to shape patterns of mitral cell firing that contribute to olfactory-related behaviors.

*Correspondence: arenkiel@bcm.edu.

AUTHOR CONTRIBUTIONS

A.M.L.-W. conducted or assisted with all experiments, analyzed data, and wrote the paper. E.T. conducted immunohistochemistry experiments and assisted with cannula placement. E.H. and M.Y.K. conducted slice electrophysiology experiments and provided input on the manuscript. B.B. conducted *in vivo* two-photon imaging experiments and provided input on the manuscript. J.O.-G. performed confocal imaging and provided assistance with viral design and production. Z.F. and B.R.A. provided intellectual guidance on experimental design, assisted with interpretation of results, and provided input on the manuscript.

SUPPLEMENTAL INFORMATION

Supplemental information can be found online at https://doi.org/10.1016/j.celrep.2023.113471.

DECLARATION OF INTERESTS

The authors declare no competing interests.

Graphical abstract

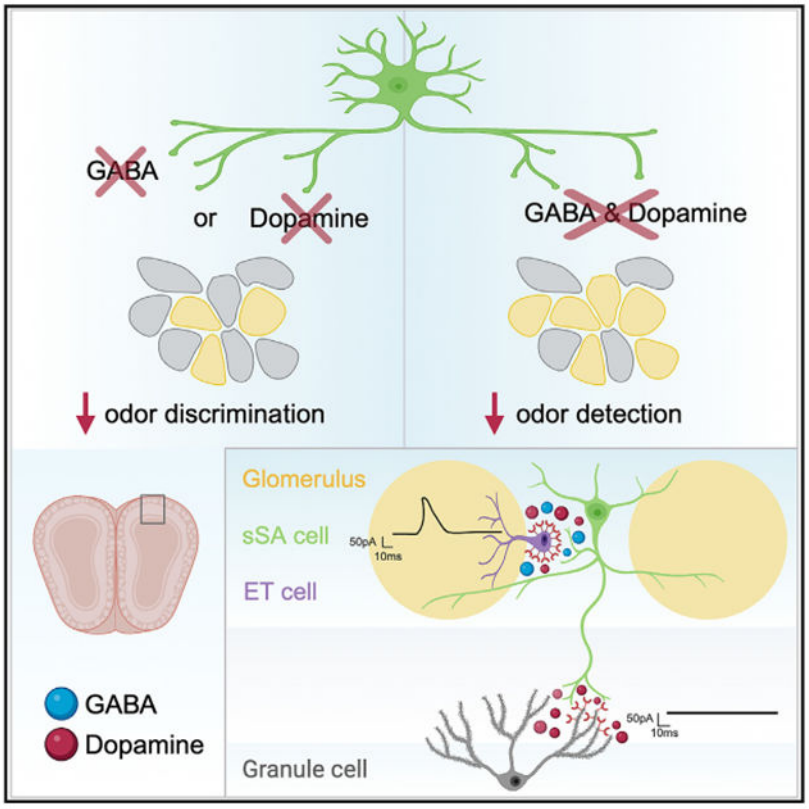

In brief

Lyons-Warren et al. selectively remove GABA or dopamine release from co-transmitting inhibitory interneurons in the olfactory bulb. They then quantify the impact on olfactory behaviors, specific target cell types, and overall odor coding, demonstrating that co-transmission can be spatially divergent with both pre- and post-synaptic regulation of distinct cell targets.

INTRODUCTION

Neurotransmitter co-transmission is increasingly recognized as a potent mechanism for dynamic regulation of neural circuits.[1] Co-transmission is a heterogeneous phenomenon in which a variety of pre- and post-synaptic mechanisms diversify neurotransmitter signaling within neural circuits.[2] For example, in the striatum, although γ-aminobutyric acid (GABA) and dopamine are packaged into the same vesicles of a single neuron,[3] differential expression of dopamine receptor subtypes leads to divergent post-synaptic effects.[4] In contrast, other co-transmitting neurons independently release neurotransmitters onto different post-synaptic targets. For example, GABAergic/histaminergic co-transmitting neurons in the tuberomammillary nucleus release GABA onto pyramidal neurons in the neocortex, but they release histamine onto the medium spiny neurons in the caudate putamen.[5] Co-transmitting cortical neurons have both overlapping and unique targets for GABA and acetylcholine, although targets that receive both signals are rare.[6] Coreleased

neuromodulators also have the potential to regulate both pre-synaptic neurotransmitter release and post-synaptic responses.[7,8] For example, co-transmission of dopamine adds opportunities for dynamic control of co-transmitted fast neurotransmitters such as GABA.[9] Thus, co-transmission is a versatile signaling mechanism that allows individual neurons to play multiple functional roles across diverse circuits by exerting distinct signaling properties of the co-released neurotransmitters.

Interestingly, GABA and dopamine colocalization has been identified throughout the brain, including in the striatum,[3] olfactory bulb (OB),[10] retina,[11] hypothalamus,[12] and cortex.[13] The role of co-transmission in the OB is particularly interesting given that co-transmitting cells and their immediate downstream targets directly contribute to early stages of olfactory processing.[14] However, the impact of superficial short-axon cell (sSAC) cotransmission on olfactory function has not been explored.

In the OB, co-transmission occurs from sSACs, which release both GABA and dopamine.[10,15] sSACs receive input from olfactory sensory neurons,[16] which also synapse onto other inhibitory and excitatory interneurons, as well as mitral cells, which are the primary output neurons of the OB.[17] External tufted cells (ETCs) are excitatory interneurons at the border of the glomerular layer that receive input from sSACs[15] and make excitatory synapses onto mitral cells.[18] Thus, sSACs are part of the initial circuitry in the bulb that first helps encode and process olfactory information. Channelrhodopsin-assisted circuit mapping has facilitated identification of many sSAC GABAergic targets,[15,19–21] including GABAergic connections onto ETCs,[15] mitral cells,[19,20] and other periglomerular inhibitory interneurons.[20–22] In contrast to targets of GABAergic signaling, those impacted by dopamine modulation have been more challenging to elucidate. Anatomical studies have supported the expression of the excitatory dopamine D_1-like receptor, D_1 (D1R), as well as the inhibitory D_2-like receptors including D_2 (D2R) and D_3 (D3R) within the OB.[23] Indeed, D2R is expressed by olfactory sensory neurons (OSNs),[24] in addition to less-defined expression in the glomerular and granule cell layers.[23,25] Also, electrophysiological recordings in slices have shown that dopamine from sSACs modulates release of glutamate from OSN terminals[26,27] as well as signaling by ETCs, periglomerular cells, sSACs, and mitral cells.[28] However, the direct dopaminergic targets of sSACs and how these relate to GABAergic targets are not well understood.

While recent progress has been made toward identifying putative targets and functions of sSAC-derived GABA and dopamine, the interaction of these two signaling mechanisms and their impact on mitral cell signaling remain largely unknown. Here, we identify distinct contributions of sSAC GABA and dopamine toward olfactory function. We provide anatomical and functional evidence for an expanded role of co-transmission by sSACs, showing GABAergic/dopaminergic signaling onto ETCs, in contrast to dopaminergic but not GABAergic signaling onto granule cells, which together directly shape patterns of mitral cell output.

RESULTS

sSAC GABA- and D1R-mediated dopamine are required for odor detection

To understand the function of sSACs toward olfactory behaviors, we investigated their role in odor detection using the buried-food test.[29] Tyrosine hydroxylase (TH) is the rate-limiting synthesis enzyme for dopamine. As sSACs are the only TH^+ cells in the OB,[30] we used TH as both a marker and cell-type-specific Cre driver. We first blocked all sSAC activity by bilaterally injecting a conditional tetanus toxin expressing virus (AAV-ef1α-DIO-TeLC-EYFP) into the OBs of *TH*-Cre mice. This manipulation selectively blocked neurotransmission from sSACs. Control animals were injected with a conditional GFP-only virus (AAV-ef1α-DIO-EYFP) (Figure 1A). Both experimental (Figures 1B, S1A and S1B) and control mice (not shown) exhibited diffuse labeling in the glomerular layer, indicating broad viral expression in sSACs. We evaluated OB slices from four experimental (mean 23.0 slices/mouse), and four controls (mean 24.8 slices/mouse) and found >50% labeling in 91% of the experimental slices and 98% of the control slices. We further confirmed virus specificity by staining for TH in these animals while enhancing the YFP signal with anti-GFP (Figures S1C and S1D). Notably, we found that the experimental cohort took significantly longer to find buried food pellets compared to control animals (Figure 1C). We therefore concluded that sSAC signaling contributes to odor detection.

Given that sSACs release both GABA and dopamine, we next asked how each of these neurotransmitters independently contribute to odor detection using the buried-food assay (Figure 2A) in mice genetically engineered to either lack dopamine (Vgat-Cre; $TH^{flox/flox}$) or GABA (*TH*-Cre;$Vgat^{flox/flox}$) release selectively from co-transmitting GABAergic/dopaminergic neurons. Surprisingly, mice singly lacking either dopamine (light green) or GABA (light blue) release from sSACs performed the same as littermate controls (dark green and dark blue) (Figure 2B). Given this result, we questioned whether developmental compensation may correct for constitutive loss of GABA release. However, there was also no difference in time to find the buried food pellet when GABA release was blocked starting at 6 weeks of age (Figure 2B). Of note, there was no difference in time to find the buried food pellet between the two $Vgat^{flox/flox}$ control groups (Figure 2B, $p = 0.3897$) or between $TH^{flox/flox}$ and $Vgat^{flox/flox}$ controls (Figure 2B, $p = 0.1439$). There was also no difference between $Vgat^{flox/flox}$ mice injected with a control GFP virus (Figure 1C) and un-injected $Vgat^{flox/flox}$ mice (Figure 2B) ($p = 0.5582$). However, we detected differences in time to find buried food between $Vgat^{flox/flox}$ mice injected with a control GFP virus (Figure 1C) and un-injected $TH^{flox/flox}$ mice (Figure 2B) ($p = 0.0031$). Adjusting for multiple comparisons, there is no change in significance ($q = 0.38$, 0.17, 0.60, and 0.08, respectively).

As the buried-food test has low sensitivity for subtle odor-detection deficits,[31] we also performed odor-detection threshold tests[32] in mice with sSACs lacking either GABA or dopamine release. Interestingly, mice lacking dopamine (Vgat-Cre; $TH^{flox/flox}$) explored odors at significantly lower concentrations compared to littermate controls, suggesting a slight improvement in odor-detection ability. We did not observe any differences between mice lacking GABA release (blue lines) and littermate controls (light blue lines, $p = 0.44$) (Figure S2A).

Having found that loss of GABA *and* dopamine, but not GABA or dopamine alone, was sufficient to cause a deficit in the buried-food test, we next examined whether the dopaminergic contribution to odor detection was mediated by D1R or D2R by genetically blocking GABA release (*TH*-Cre;Vgat$^{flox/flox}$) while also pharmacologically blocking D1R or D2R receptor signaling via subcutaneous injection of either the D1R-specific antagonist SCH39166 or the D_2-like-receptor-selective antagonist L-741,626 (Figure 2A). In this way, we attenuated GABA synthesis, leaving only dopamine release from sSACs and then selectively blocked either D1R or D2R signaling to identify which dopamine receptor contributed to impaired odor detection in mice lacking all sSAC signaling (Figure 1). Interestingly, we observed a significant increase in time to find a buried food pellet in mice lacking GABA release with concomitant D1R blockade. In contrast, we found no effects in mice lacking GABA release from sSACs alongside D2R inhibition (Figure 2C). We also found differences in time to find buried food pellets between Vgat$^{flox/flox}$ control mice with or without viral injection and Vgat$^{flox/flox}$ control mice that received a D1R ($p = 0.0027$) or DR2 blocker ($p = 0.0368$), likely due to broader systemic impact of the dopaminergic blockade. To confirm that the increased time to find buried food was not due to off-target effects, we repeated the pharmacology experiment with drug infusion directly to the OB via intracranial catheters. Again, we observed a significant increase in time to find a buried food pellet in mice lacking GABA release and concomitant D1R inhibition ($p = 0.0103$). We observed no effects in mice lacking GABA release from sSACs alongside D2R inhibition ($p = 0.3969$). Importantly, there were also no differences between groups following infusion of saline ($p = 0.7430$). (Figure S2B). Thus, we concluded that sSACs contribute to odor detection via GABA and D1R-mediated dopamine signaling.

sSAC GABA and dopamine are necessary for odor discrimination

Having found that sSAC signaling contributes to odor detection, we next asked whether it also impacts odor discrimination. Since complete loss of sSAC signaling dramatically impaired odor detection, we first evaluated odor discrimination in mice lacking either GABA or dopamine release selectively from co-releasing GABAergic/dopaminergic neurons. For this, we used a habituation/dehabituation paradigm to test odor discrimination ability (Figure 2D). Interestingly, both mice lacking dopamine release from sSACs (Figure 2E, green) and those lacking GABA release from sSACs (Figure 2E, blue) showed impaired discrimination between anisole and acetophenone. In contrast, controls easily discriminated between these odorants. Moreover, we observed similar discrimination deficits when testing isoamylacetate (IAA) from isoamylbuturate (IAB) (Figure 2F). Importantly, all mice tested exhibited no preference during the third habituation trial (Figures S2C–S2E). To further assess odor discrimination ability, we next measured learned odor discrimination using a go-no-go olfactory task.[33] After demonstrating the ability to learn the task, mice were challenged with three odor pairs of varying difficulty: (1) IAA vs. IAB, (2) pentanol vs. hexanol, and (3) S+ vs. S− carvone. No differences in odor discrimination as measured by D prime were observed for either control or experimental groups (Figure S2F). Thus, we concluded that sSAC GABA and dopamine both contribute uniquely to spontaneous but not learned odor discrimination.

Co-transmitting GABAergic/dopaminergic neurons also exist outside of the OB.[13,34,35] Given the improvement in odor-detection ability for mice lacking dopamine release, we next asked whether this finding was due to selective loss of dopamine from sSACs or whether other co-transmitting GABAergic/dopaminergic neurons in the brain could be contributing. Toward this, we bilaterally injected the OBs of Vgat-Flp;*TH*$^{flox/flox}$ mice with a Flp-dependent Cre virus and then assessed odor detection using buried food (Figure S2G) while also incorporating odor-detection threshold measurements (Figure S2A). As we previously observed for Vgat-Cre;*TH*$^{flox/flox}$ animals, we observed no differences in time to find buried food. Notably, *TH*$^{flox/flox}$ control mice from both this and earlier experiments exhibited almost identical performances on the odor-detection tasks (green solid lines, open and closed circles). We noted a trend toward earlier exploration times in our Cre-injected mice, although these were not significantly different from controls ($p = 0.06$). We also performed odor discrimination assays in Vgat-Flp;*TH*$^{flox/flox}$ and *TH*$^{flox/flox}$ littermate controls injected with Flp-dependent Cre viruses. Again, we found that *TH*$^{f/f}$ littermate controls were able to discriminate both IAA vs. IAB and anisole versus acetophenone, while Vgat-Flp;*TH*$^{flox/flox}$ mice could not (Figure S2H). Similar to Vgat-Cre;*TH*$^{flox/flox}$, we observed no differences in learned odor discrimination for (1) IAA vs. IAB, (2) pentanol vs. hexanol, or (3) S+ vs. S− carvone (Figure S2I).

D1R-mediated dopamine enhances sSAC inhibition of ETCs

Having shown that sSAC GABA and dopamine contribute to both odor detection and odor discrimination, we next wanted to better understand the circuit properties underlying how sSACs impact these behaviors by identifying the GABAergic and dopaminergic targets of sSACs. Previous work[15] suggested that sSACs make GABAergic, inhibitory connections onto ETCs. We confirmed this connection using channelrhodopsin-assisted circuit mapping (CRACM). Toward this, we made whole-cell recordings from ETCs, initially identified based on anatomical shape and location, while evoking GABA release from sSACs in *TH*-Cre;LSL-ChR2 mice (Figure 3A). Cell identity was subsequently verified via *post hoc* imaging of biocytin cell fills (Figure 3B). Through these recordings, we identified monosynaptic, GABAergic synapses from sSACs onto 70% (12 out of 17) of recorded ETCs (Figure 3C), which exhibited mean amplitudes of 166.7 ± 75.36 pA, mean peak times of 15.56 ± 1.35 ms, mean onset latencies of 4.89 ± 0.62 ms, and mean halfwidths of 365 ± 123 ms.

Based on our finding that D1R but not D2R signaling mediated odor detection, we next evaluated the anatomic localization of D1R within the bulb. While we focused on the potential role of D1R given results from pharmacological blockade, prior work using *in situ* hybridization and radioligand binding suggested D1R, D2R, and D3R are all present in the OB.[23]

As previous studies did not report the identity of the cells expressing dopamine receptor subtypes, we used a genetic marker to determine which cell types in the OB expressed D1R. Specifically, we imaged OB tissue from Drd1a-tdTomato^{tg} transgenic mice[36] and observed diffuse labeling in the glomerular, mitral cell, and granule cell layers (Figure 3D), suggesting that D1R-expressing cells are present throughout the OB. Notably, the position

of D1R-expressing cells at the border of the glomerular and external plexiform layer was consistent with the location of ETCs (Figure 3D, arrow). The 40-μm OB slices from Drd1a-tdTomato^{tg} mice stained for the neuropeptide cholecystokinin (CCK) showed colocalization, further supporting that ETCs express D1R (Figures S3A and S3B). Double-fluorescence *in situ* hybridization for tdTomato and D1R in the OB of Drd1a-tdTomato^{tg} mice revealed diffuse colocalization, suggesting endogenous D1R expression is preserved (Figure S3C).

To directly test whether D1R-expressing ETCs at the border of the glomerular and external plexiform layers were the same population that received sSAC GABAergic inhibition, we repeated CRACM recordings in brain slices from mice with labeled D1R-expressing cells (*TH*-Cre;LSL-ChR2;Drd1a-tdTomato). For these experiments, we photostimulated sSACs while recording GABAergic responses from D1R-positive cells at the border of the glomerular and external plexiform layers of the OB (Figure 3E). We observed monosynaptic GABAergic currents from six out of six red-labeled neurons that we confirmed to be ETCs via *post hoc* biocytin staining to visualize cell identity (Figures 3F and 3G).

Having shown that D1R-expressing ETCs received GABAergic input, we next examined how monosynaptic connectivity between sSACs and ETCs may be modulated by dopamine. For this, we recorded from ETCs while stimulating sSACs (Figure 3A) before and after application of D1R blocker SCH39166. Following application of SCH39166, peak amplitudes of evoked inhibitory post-synaptic currents (IPSCs) in ETCs decreased significantly (Figures 3H and 3I). Application of SCH39166 also decreased the amplitudes of spontaneous IPSCs on ETCs (Figure 3I). Together, these data suggest that dopamine affects ETCs both directly and indirectly. In contrast, following application of the D2R antagonist sulpiride, peak amplitudes of evoked IPSCs in ETCs did not change (Figure 3J). Recorded ETCs across both experiments exhibited a mean membrane resistance of 150.625 ± 20.8 MOhm and mean capacitance of 83.125 ± 7.48pF. Finally, we recorded baseline firing frequencies of ETCs in mice lacking GABA or dopamine release from sSACs. In the absence of GABA, ETC firing rate was significantly less than observed in litter mate controls (Figure S3D). We noted a similar trend in mice lacking dopamine, but it was not significant (Figure S3E). Together, these data suggest that ETCs receive both GABAergic and dopaminergic input from sSACs and that sSAC dopamine serves to augment GABAergic signaling. Notably, although L-741,626 was used for D2R-specific blockade *in vivo* via subcutaneous injection, sulpiride was chosen as the D2R antagonist for slice electrophysiology and direct infusion based on prior work in the bulb.[15]

Granule cells receive dopaminergic but not sSAC GABAergic input

Using Drd1a-tdTomato^{tg} transgenic mice, we observed diffuse labeling in the glomerular, mitral cell, and granule cell layers (Figures 3D and 4A). Interestingly, D1R-expressing cells in the mitral cell layer co-labeled with 5T4, a granule cell subtype marker[37] (Figure 4A), but not the mitral cell marker Tbx-21[38] (Figure 4B). Quantifying 5T4 labeling of Drd1-tdTomato cells within the mitral cell and granule cell layers in OB slices from three animals, we found approximately half of D1R^{+} cells were positive for 5T4 (52.6% ± 8%, 50.3% ± 4%, and 37.5% ± 4% counting three slices from each animal; representative images in Figure S4). Thus, we concluded that granule cells—but not mitral cells—express D1R.

To determine whether dopamine receptors on granule cells were functional, we next performed voltage-clamp recordings from D1R-expressing granule cells before and after application of increasing concentrations of dopamine (Figure 4C). Indeed, D1R-expressing granule cells exhibited slow depolarizing currents with an amplitude of 7.7 ± 2.2 pA in the presence of bath-applied 10 μM dopamine (n = 6 cells; Figure 4D). This change was dose dependent, with an amplitude of 8.5 ± 2.8 pA in the presence of 100 μM dopamine (n = 10 cells; Figure 4E). We observed no changes in amplitude following application of saline (0.5 ± 0.8 pA, n = 6 cells) or 1 μM dopamine (1.0 ± 1.4 pA, n = 5 cells) (Figure 4E).

To further evaluate sSAC inputs onto granule cells, we injected two *TH*-Cre mice with viruses expressing a Cre-dependent myc-labeled VMAT (AAV-EF1α-DIO-VMAT2-myc) to label monoaminergic terminals, as well as a Cre-dependent V5-labeled VGAT (AAV-EF1α-DIO-VGAT-V5) to label GABAergic terminals. To visualize these reporters, we prepared 25-μm slices and stained for both V5 and myc. As expected, we observed extensive labeling of both V5 and myc in the glomerular layer (Figure 4F) but observed only myc and not V5 labeling in the granule cell layer (Figure 4G). Next, we injected these same viruses plus a Cre-dependent cell fill (AAV-EF1α-DIO-tdTomato) bilaterally into OBs of a TH-Cre mouse. We observed tdTomato-labeled TH+ cells extending from the glomerular layer to the granule cell layer with $VMAT2^+$ but not $VGAT^+$ puncta (Figure S5A). Finally, we injected these same viruses into TH-Cre;Drd1a-tdTomato^{tg} mice and evaluated the relationship of VMAT2 and VGAT expression in the granule cell layer to D1R expressing cells. Indeed, we saw robust VMAT2, but not VGAT, labeling surrounding $D1R^+$ cells (Figure S5B). Thus, both pre- and post-synaptic evidence supported sSAC dopaminergic, but not GABAergic, signaling onto granule cells.

As D1R-expressing ETCs were identified to receive GABAergic input from sSACs, we next asked whether other D1R-expressing cells receive GABAergic input from sSACs. Using *TH*-Cre;LSL-ChR2;Drd1a-tdTomato^{tg} mice, we recorded from D1R-expressing granule cells while stimulating sSACs (Figure S5C). None of the D1R-expressing granule cells exhibited GABAergic currents in response to sSAC stimulation (Figure S5D), although clear responses were seen in ETCs from these animals (Figure 3G). Thus, D1R-expressing granule cells responded to dopamine but did not receive monosynaptic GABAergic inhibition from sSACs. While we cannot rule out additional extrabulbar sources of dopamine, sSACs represent a prime candidate for dopaminergic modulation of granule cells, suggesting a model in which sSACs differentially utilize GABAergic and dopaminergic signaling on their downstream targets.

sSAC GABA and dopamine both exert a net effect to decrease mitral cell firing

Mitral and tufted cells represent the projection neurons from the OB to the piriform cortex and anterior olfactory nucleus and thus carry all odor information from the bulb.[39,40] Having found divergent GABAergic and dopaminergic targets of sSACs signaling, we next examined how these circuit connections impact mitral cell firing. We hypothesized that loss of either GABA or dopamine would increase mitral cell activity. To test this hypothesis, we used OB slice electrophysiology and recorded spontaneous firing rates in mitral cells from mice lacking either GABA (TH-Cre;Vgat$^{flox/flox}$) or dopamine (Vgat-Cre;TH$^{flox/flox}$)

release selectively from co-transmitting GABAergic/dopaminergic neurons (Figure 5A). Indeed, we observed a significant increase in spontaneous mitral cell firing rates for TH-Cre;Vgat$^{flox/flox}$ mice compared to VGAT$^{flox/flox}$ littermate controls (Figures 5B and 5D); these differences were also reflected via interspike intervals when comparing Vgat-knockout animals versus controls (Figures 5C and 5D). While we observed no change in spontaneous mitral cell firing for Vgat-Cre;*TH*$^{flox/flox}$ compared to *TH*$^{flox/flox}$ control animals (Figures 5D and 5E), interspike intervals were altered (Figures 5D and 5F). Notably, the rightward shift in the interspike interval curve indicated that loss of dopamine led to more even patterns of mitral cell firing, combined with a decrease in likelihood of achieving high frequencies; these observations were distinct from the absolute increase in mean firing rate observed in mice lacking GABA release. Thus, we concluded that loss of GABA or dopamine signaling from sSACs impacts mitral cell firing rates, albeit in different ways.

Having identified that loss of GABA release from dopamine/GABA co-transmitting sSACs led to an increase in spontaneous mitral cell firing, we next asked how loss of either signaling pathway impacted odor-evoked mitral cell responses *in vivo*. Informed by our prior *in vitro* recording experiments, we posited that loss of GABA but not dopamine would elevate odor-evoked mitral cell activity. To test this, we performed *in vivo* two-photon imaging of the OB in mice expressing Thy1GCamp6f to record mitral cell activity at glomeruli during odor presentation using a multi-channel constant-flow olfactometer[41] (Figure 6A). High-spatial-resolution imaging allowed confirmation of glomerular location (Figure 6B). Based on these images, standardized regions of interest (ROIs) were placed in the center of each glomerulus to measure changes in fluorescence over time. Response data were then collected during presentation of 10 randomized odors plus mineral oil control. For each odor presentation, a total of 20 s of activity were recorded, including 10 s of baseline, 2 s of odor presentation, and 8 s of response (Figure 6C). Each odor, including mineral oil, was presented three times during the recording period in a randomized order, and the three independent responses were averaged. In some glomeruli, we observed a non-specific response to mineral oil. Therefore, we subtracted the averaged mineral oil response from each odor response to establish a baseline for odor-specific responses. A glomerulus was considered to have responded to an odor if the change in fluorescence during the 2-s odor presentation window exceeded 4 SD of baseline activity (Figure 6C, stars). Mean numbers of glomeruli per recording session were 10.5 for Vgat-Cre;*TH*$^{flox/flox}$;Thy1GCamp6f and *TH*$^{flox/flox}$;Thy1GCamp6f mice, 10.7 for *TH*-Cre;Vgat$^{flox/flox}$;Thy1GCamp6f, and 10.9 for Vgat$^{flox/flox}$;Thy1GCamp6f mice.

Similar to *in vitro* slice recordings, we found that glomeruli in mice lacking GABA release from sSACs (*TH*-Cre;Vgat$^{flox/flox}$;Thy1GCamp6f) responded to more odors compared to littermate controls (Vgat$^{flox/flox}$;Thy1GCamp6f) (Figure 6D). Notably, however, there was no difference in the magnitude of responses as measured by area under the curve for the three odors with the greatest number of responsive glomeruli (Figure 6E). Mean areas under the curve for all odors tested are listed in Table S1.

Interestingly, in mice lacking dopamine release from sSACs (Vgat-Cre;*TH*$^{flox/flox}$;Thy1GCamp6f), measured glomeruli also responded to more odors compared to littermate controls (*TH*$^{flox/flox}$;Thy1GCamp6f) (Figure 6F). There was again no difference in

the magnitude of responses as measured by area under the curve for any odorants (Figure 6G). In summary, we found that loss of GABA or dopamine from sSACs increased the likelihood that any individual glomerulus would respond to any given odor, changing the spatial response pattern across the bulb. In contrast, our manipulations did not affect the magnitude of responses. Thus, we concluded that loss of GABA or dopamine led to selective alteration in spatial activation patterns in the OB.

DISCUSSION

Here, we have uncovered the roles of GABAergic-dopaminergic co-transmission from sSACs in the olfactory circuitry. We provide evidence supporting a model in which sSAC GABA- and D1R-mediated dopamine signaling contributes to odor detection and odor discrimination through modulation of mitral cell firing via co-transmission onto ETCs, in contrast to dopaminergic mediation of granule cell firing (Figure 7). Recent work suggested that dopamine-GABAergic juxtaglomerular neurons could be divided into five subgroups,[42] but the functional relevance of these subgroups is unknown as studies to date have utilized TH as a unique marker of sSAC. Thus, this work builds on prior studies[15,19,20] that evaluated the glomerular layer circuits of the OB by uncovering divergent signaling patterns from TH+ sSACs.

Combining multiple complementary genetic tools, we showed that D1R-expressing ETCs receive GABAergic input from sSACs, while D1R-expressing granule cells do not. Thus, our data provide evidence for divergent targeting in which sSACs differentially utilize GABA and dopamine, sometimes together and sometimes separately. Co-transmitting neurons use many different mechanisms to segregate their targets.[2,8] Such divergent signaling described here may be considered similar to what occurs in the retina, where co-transmitting starburst amacrine cells differentially release acetylcholine with or without GABA onto direction-selective ganglion cells based on the directionality of incoming light.[43,44]

Our results further support prior studies in which optical stimulation of sSACs four to five glomeruli away led to GABA-mediated inhibition, followed by rebound excitation of ETCs.[15] In the same study, stimulation of sSACs also produced small (5 pA) inward currents in ETCs, which were also present following application of dopamine or D1R agonists and were blocked following application of D1R and D2R antagonists. Recent work evaluating the role of dopamine in the glomerular layer of the OB proposed that sSAC dopamine modulates ETC excitation onto mitral cells via D1R and D2R.[28] However, we found that sSAC inhibition of ETCs is modulated by D1R but not blockers of D2-like receptors (Figure 3). Notably, olfactory sensory neurons have been shown to express D2 receptors, which influence olfactory behaviors via dopamine in the olfactory epithelium, suggesting that receptors are expressed on the cell body.[32] The functional relevance of D2-like receptors expressed on olfactory sensory neuron projections and/or other cell types in the glomerular layer is not well understood. Thus, direct evaluation for D2R and D3R cell-type-specific expression in the bulb will be necessary to clarify which other receptors are involved. Interestingly, broad glomerular application of exogenous dopamine without stimulation of sSACs resulted in a short-term net excitatory effect onto mitral cells, which

was proposed to be mediated by increased ETC excitation of mitral cells.[28] Our data suggest that dopamine could in fact impact mitral cells via multiple pathways. Thus, in the OB, divergent co-transmission allows a single cell type to differentially modulate their respective targets.

Elucidating sSAC signaling mechanisms is important for understanding how olfactory information is encoded within the initial stages of olfactory circuitry. Strikingly, little is known about how sSACs contribute to olfactory-related behaviors. sSAC activity increased with odor concentration,[45] suggesting that they contribute to odor sensitivity. Further, mice lacking dopamine signaling throughout the brain, based on knockout of either D2R or the dopamine transporter, exhibited impaired odor discrimination.[46] This is similar to our model in which blocking dopamine release exclusively from dopamine/GABA co-transmitting neurons (Figure 2) impaired odor discrimination. Indeed, we showed evidence (Figures 1 and 2) to support an essential role for sSACs in both odor detection and odor discrimination.

Notably, mitral and tufted cells carry odor information from the OB to cortical structures[39,40] and thus serve as a readout of olfactory processing. However, the impact of increasing or decreasing mitral cell activity on olfactory function is complex. For example, odor discrimination improved in mice with *decreased* mitral cell activity via increased granule cell inhibition.[47] In contrast, recent work in which all mitral cell activity was *increased* through targeted loss of Kv1.3 channels also led to improved odor discrimination.[48] Together, these data suggest blanket increases or decreases in mitral cell activity do not explain how odor information is encoded. Rather, we show that loss of either sSAC GABA or dopamine impacted mitral cell firing frequency (Figure 5) and increased the number of glomeruli that responded to a given odor (Figure 6). Together, this led to impaired odor discrimination (Figure 2). Of note, we did not investigate the contributions of other key cell types in the OB, including periglomerular cells or olfactory sensory neurons, which also contribute to olfactory processing. Thus, loss of GABA or dopamine from sSACs could have more widespread impacts on olfactory function via these circuit components as well.

Importantly, while we observed an increase in spontaneous mitral cell firing following loss of GABA release from sSACs (Figure 5B), we found no change in the amplitude of glomerular responses during *in vivo* imaging of odor-elicited activity (Figures 6E and 6G). In contrast, we found an increase in the number of odors that any given glomerulus responded to (Figures 6D and 6F), suggesting that gain control was intact, but the patterns of odor responses were disrupted (Figure 6). This interpretation fits well with prior work suggesting that odor discrimination relies on sparse patterns of mitral cell firing, where increasing the number of olfactory sensory neurons that respond to the same odor impaired rather than improved odor discrimination.[49] Further, a model of sparse sSAC inhibition better reflected other models of odor coding.[50]

Also, it is well known that mitral cells are directly modulated via granule cells,[51] which are necessary for odor discrimination.[52] Our data show that granule cells express D1R and are modulated by dopamine. Interestingly, loss of 5T4-expressing cells, a marker associated with granule cells, resulted in odor-detection deficits.[53] Similarly, administration of the D1R agonist SKF 38393 has been shown to improve odor detection in rats.[54] Together, these

data suggest that dopamine signaling via D1R enhances odor detection and discrimination. On the other hand, application of the D2R/D3R agonist quinpirole to rats impaired odor detection in a dose-dependent manner.[55] Taken together, these studies substantiate that further work is needed to evaluate the cell-type-specific localization of D2R and D3R in the OB.

Limitations of the study

This work has several limitations to consider. First, it is important to recognize that our genetic manipulations impacted all GABAergic-dopaminergic neurons in the brain, including those outside the OB. We addressed this limitation through viral-mediated, bulb-specific manipulation of dopamine release, which is more specific but less sensitive, as not all sSACs will be infected. Thus, we cannot exclude the possibility that GABAergic/dopaminergic co-transmitting cells outside the OB contribute to odor discrimination. Relatedly, while sSACs are the only dopaminergic neurons in the bulb, some evidence suggests that dopaminergic projections that innervate the OB may originate from central sources such as the striatum.[56] Thus, we cannot fully confirm that the identified dopamine receptors exclusively respond to only local dopamine or that changes observed in response to dopaminergic blockers fully reflect manipulation of locally acting dopamine. While our OB slice preparation does not include intact projections from the striatum, terminals are still present, and thus ambient dopamine from this source cannot be excluded. Importantly, we only assessed the impact of sSAC signaling on specific target populations. Other cell types, including mitral cells, may also receive GABAergic and/or dopaminergic input from sSACs, the contributions of which were not investigated in this study. Similarly, this study used 5T4 staining as a marker for granule cells to understand which cells expressed DRD1 receptors but did not directly investigate whether sSAC interact electrophysiologically with 5T4+ cells in the granule or periglomerular cell layers. Finally, we found significant differences in odor detection as measured by both the time to find buried food and odor-detection threshold tasks between $TH^{flox/flox}$ and $Vgat^{flox/flox}$ controls. We hypothesize that this is because these lines are maintained on different genetic backgrounds, underlying the multifactorial contributions to olfactory behaviors, which limits the generalizability of mouse behavior testing.

Conclusions

In sum, the work presented here provides evidence of co-transmission by sSACs via GABAergic synapses onto D1R-expressing ETCs, and an absence of GABAergic signaling onto dopamine receptor-expressing granule cells. Separating the distinct contributions of sSAC GABA and dopamine and their impacts on mitral cell activity provides two key conclusions. First, dopamine acts in concert with GABA through multiple pathways to balance odor detection and discrimination. Using mouse olfaction as a model, this work informs how neuromodulation can sculpt distinct sensory features. Notably, similar mechanisms are likely acting in other sensory modalities. Second, circuit changes that impact the overall gain of mitral cell activity increase the sensitivity of olfactory function. However, odor processing in the bulb relies on stimulus-specific patterns of mitral cell activation, which are modulated by co-transmitting sSACs to improve odor detection and

discrimination. Overall, while increased mitral cell gain improves odor discrimination, we also found that disruption of mitral cell patterning impairs odor discrimination and that sSAC GABA and dopamine work together to modulate patterns of mitral cell firing. Given that co-transmission is becoming more evident in many cell types throughout the brain, future studies will need to account for differential effects of multiple neurotransmitters from the same source on circuit function.

STAR★METHODS

RESOURCE AVAILABILITY

Lead contact—Further information and requests for resources and reagents should be directed to and will be fulfilled by the lead contact, Benjamin Arenkiel (arenkiel@bcm.edu).

Materials availability—The three plasmids generated in this study are available through the IDDRC Neuroconnectivity Core at Baylor College of Medicine via the following link:

https://forms.office.com/Pages/ResponsePage.aspx?id=UHZPhkXFdE-aK7VHBcA1d8_crwdaG-dCsrC43WWsNdxURFYyMEVCTDdKN1pVWEtMVFBSMlQxNVE2SS4u.

AAV-ef1a-DIO-TeLC-EYFP.

AAV-EF1a-DIO-VGAT-V5.

AAV-ef1a-FlpDIO-Cre.

Data and code availability

- All data reported in this paper will be shared by the lead contact upon request.
- This paper does not report original code for data analysis. In-house MATLAB code for triggering image acquisition timed to odor presentation specific to our imaging set up is available upon request.
- Any additional information required to reanalyze the data reported in this work paper is available from the lead contact upon request.

EXPERIMENTAL MODEL AND STUDY PARTICIPANT DETAILS

Adult mice including equal numbers of both sexes were used for all experiments.

Mice were housed in a standard 12-h light/dark cycle and had *ad libitum* access to food and water. Standard breeding and genotyping schemes were used to identify desired genotypes. Genotyping primers and protocols were used as provided by Jax. All experimental procedures were approved by the Baylor College of Medicine Institutional Animal Care and Use Committee.

METHOD DETAILS

Olfactory behavior experiments—Odor detection was evaluated using a "buried food" assay.[29] Briefly, mice were habituated to the test chamber for 15 min per day for three days. Following the third habituation period, they were food restricted for 24 h. On test day, a standard chow food pellet was buried just below the surface of the bedding at one end of the test chamber. Mice were placed in the center of the test chamber and the time until the finding the buried food pellet was measured. Odor detection was also measured using an odor detection threshold assay.[32] Briefly, habituated mice were placed in a chamber with a tea diffuser containing only mineral oil. Every 2 min, the tea diffuser was replaced with a new tea diffuser containing R-limonene dissolved in mineral oil at concentrations ranging from zero to 10^{-4}. Time spent sniffing the tea diffuser defined as the nose within 1 cm of the diffuser was quantified as an indication of odor detection.

Spontaneous odor discrimination was evaluated using a habituation/dehabituation assay.[62] Briefly, mice were habituated to the test chamber for 15 min per day for three days. On the day of the experiment, mice were further habituated first to the empty test chamber for 5 min and then to the test chamber with blank tea diffusers for 5 min. Removable walls dividing the chamber into three compartments were then placed, restricting the mouse to the middle chamber. A tea diffuser with 20 mL of 0.5% odor in mineral oil on gauze was placed in the center of each side chamber, a recording camera was started, and the walls were removed. Every 2 min, the removable walls were inserted, the tea diffusers were replaced, and the walls were removed for a total of four 2-min trials. During the first three trials, both tea diffusers contained odor 1 (acetophenone or isoamylacetate). During trial four, one tea diffuser contained odor 1 and the other contained odor 2 (anisole or isoamylbutyrate). The side containing the novel odor was alternated to avoid bias. Video was captured at 10 frames per second using a Doric behavior tracking camera with 1920x1080 resolution. Mouse position in the video was analyzed using Optimouse MATLAB software.[63] Learned odor discrimination was tested using an olfactory go-no-go task.[33]

For pharmacology experiments, subcutaneous injections of 0.002 mg/kg SCH 39166 or 0.015 mg/kg L-741,626 dissolved in DMSO were performed 1 h before behavioral assessment. For intracranial infusions, 0.5 mm depth Y cannulas spaced 1.5mm apart were placed into olfactory bulbs of 9 *Vgat*$^{flox/flox}$ and 8 *TH*-Cre;*Vgat*$^{flox/flox}$ mice. Mice were allowed to recover for 2 weeks prior to testing. On test day 0.05 mL of either sterile saline, 10 μM SCH 39166, or 100nM Sulpiride was infused into each bulb under isofluorane anesthesia over 15 min. Buried food testing was performed as soon as the mice demonstrated ambulation (average time from infusion to testing 24.4 ± 1.34 min).

Immunohistochemistry—Briefly, animals were euthanized using isoflurane and then perfused through the heart with 10 mL phosphate buffered saline (PBS) followed by 10 mL 4% paraformaldehyde (PFA). Dissected brains with intact olfactory bulbs were fixed overnight in 4% PFA at 4°. Brains were then transferred to 30% sucrose for at least 24 h prior to embedding in optimal cutting temperature (OCT) (Fisher Scientific) for cryostat sectioning. 25 or 40 μm sagittal slices through the olfactory bulb were collected from each animal. All slices were mounted with Fluoromount-G (Southern Biotech 0100–200) and

imaged on an upright confocal microscope. For counter-staining, slices were rinsed with fresh PBS with 10% Triton X-, incubated in blocking solution for 2 h at 4°, and incubated overnight at 4° with primary antibody. After primary antibody incubation, slices were rinsed five times with PBS for 5 min each and then incubated for 2 h at room temperature with secondary antibody (Alexa Fluor 488 or 633). Slices were then rinsed four times for 5 min each in PBS, mounted and imaged as stated above. Double fluorescent *insitu* hybridization was performed by a core facility at our institution.

Stereotaxic microinjection of adeno-associated viruses—Stereotaxic injections into the mouse olfactory bulb were done as previously described.[64] Briefly, hair was removed from the dorsal scalp using a handheld electric shaver. Mice were then head fixed using ear bars and positioned to receive continuous anesthesia with isoflurane. Each animal received 5 mg/kg pre-operative subcutaneous Meloxicam for pain control and protective ointment was placed on eyes to prevent drying. A small, incision was made in the scalp to expose the olfactory bulbs. A single burr hole was created in the skull above the center of each olfactory bulb. 3.5″ Drummond pipette glass (Drummond Scientific, #3-000-203-G/X) was pulled to a fine tip and used to inject virus. The pipette was stereotaxically lowered 0.90 mm and 345 nL of virus was injected. The electrode was then raised to 0.65 mm and another 345 nL of virus was injected. The electrode was removed, the scalp was sutured closed, and the animals were allowed to recover for at least 2 weeks.

In vitro electrophysiology—Brain slicing, whole-cell electrophysiology, and optogenetic circuit mapping were performed as previously described.[65] For brain slicing, mice were deeply anesthetized with isoflurane then transcardially perfused with ice-cold artificial cerebrospinal fluid (aCSF) solution containing (in mM): 125 NaCl, 2.5 KCl, 1.25 NaH_2P0_4, 1 $MgCl_2$, 2 $CaCl_2$, 25 glucose, and 25 $NaHCO_3$ (pH 7.3, 295 mOsM). Brains were removed and transferred into ice-cold cutting solution containing (in mM): 2.5 KCl, 1.25 NaH_2PO_4, 10 $MgSO_4$, 0.5 $CaCl_2$, 234 sucrose, 11 glucose, and 26 bicarbonate. Cutting solution was continuously bubbled with 95% CO2/5% O_2. Prior to slicing, brains were embedded in 1.5% low melting point agarose. Agar-embedded brains were immediately submerged in oxygenated cutting solution on a Leica VT1200 vibratome. 300 μm coronal sections were made at a cutting speed of 0.4 mm/s. Slices were removed to a slice recovery chamber of oxygenated aCSF at 37°C for at least 30 min. Following recovery, slices were slowly returned to room temperature for 30 min before recording.

For whole-cell voltage-clamp recordings, slices were submerged in a recording chamber and continuously perfused with room temperature oxygenated aCSF at ~2 mL/minute. Unlabeled external tufted cells and mitral cells were visualized with DIC optics (Olympus BX50WI) and identified by their location within the OB and their unique morphologies. D1R-expressing external tufted cells and granule cells were identified with fluorescence imaging then visualized for whole-cell recording using DIC optics. Once visualized, cells were whole-cell patched in voltage-clamp configuration. Recording electrodes (3–7 MΩ) were pulled from thin-walled borosilicate glass capillaries (inner diameter: 1.1 mm, outer diameter: 1.5 mm) with a horizontal micropipette puller (Sutter Instruments). Voltage-clamp internal solution contained (in mM): 120 Cs Methanesulfonate, 6 CsCl, 20 HEPES, 1 EGTA,

0.2 MgCl2, 10 phosphocreatine, 4 MgATP, 0.4 NaGTP (with 0.2–0.4% biocytin by weight, pH to 7.3 with CsOH, 285 mOsM). Recordings were made using PClamp software (Axon) with an Axon MultiClamp 700B amplifier digitized at 10 kHz (Axon Digidata 1440A). Traces were filtered offline in Clampfit (Axon) with a Gaussian lowpass filter then exported for processing and analysis with custom MATLAB scripts.

For optogenetic circuit mapping, patched cells were first voltage-clamped at −65 mV to record baseline membrane properties. To check for the presence of light-evoked inward currents, channelrhodopsin was activated by full-field illumination from a filtered xenon light source (Olympus, U-N41020). The onset and duration of light stimulation was controlled through ClampEx software by a mechanical shutter (Sutter). Following voltage clamping at −65 mV, patched ETCs and GC were then voltage-clamped at 0 mV (adjusted for junction potential) to reveal outward currents. If a light-evoked outward current was observed in aCSF, then TTX (1 mM), 4AP (0.5 mM), and bicuculline (BIC, 10 mM) were serially bath-applied to verify (1) the action potential-dependence, (2) the monosynaptic nature, and (3) the GABA receptor-dependence of the evoked current. All cells were dialyzed with 0.15–0.4% biocytin for the duration of the recording and patched neurons were saved for post hoc staining, imaging and reconstruction. After recordings, electrodes were withdrawn slowly, allowing the cells to reseal and form an outside-out patch. Slices were then allowed to equilibrate in the recording chamber for 5 min before being transferred to 4% PFA.

For imaging biocytin cell fills, slices were incubated in 4% PFA overnight and then washed in PBS for 30 min. Slices were then incubated in 10% normal goat serum blocking buffer for 2 h at room temperature before being transferred to blocking buffer including Streptaviden-Alexa647 (1:500) and incubated overnight at 4°C. Following overnight incubation, slices were washed 3 times in PBS for 30 min then mounted on slides with a 300 μm spacer in glycerol mounting media. Cell fills were imaged on an upright Leica SPE confocal with a 10× air objective. Z stacks were taken along the entire observed depth of the filled cell at 1.5 μm intervals and maximum values were Z-projected to obtain the final images.

For pharmacology experiments, the D1R-specific antagonist SCH 39166 or the D2R specific antagonist Sulpiride was bath applied at 10 mM or 100 mM respectively dissolved in DMSO. To assess functionality of dopamine receptors on granule cells, dopamine was bath applied at 1, 10 or 100 mM dissolved in DMSO.

2-Photon imaging—Cranial windows over the olfactory bulb were created using a modified version of a previously described protocol.[66] Briefly, hair was removed from the dorsal scalp using a handheld electric shaver. Mice were then head fixed using ear bars and positioned to receive continuous anesthesia with isoflurane. Each animal received 5 mg/kg pre-operative subcutaneous Meloxicam and 1 mg/kg Bupenorphine SR for pain control and protective ointment was placed on eyes to prevent drying. The scalp was removed to expose the skull which was cleaned and dried. Dental cement was used to affix a 0.0.16″ thick stainless steel shortening shim (ID .314”, OD 0.438” McMaster-Carr part number A370-974) over the olfactory bulb. A 3mm ring centered over the olfactory bulb was drilled through the skull and the skull “cap” was lifted out. The dura was carefully removed. A 3

mm glass coverslip (Warner instruments catalog # 64–0720) was placed over the exposed brain and glued in place first with vetbond and then with Loctite superglue. Once dry, the coverslip was protected with Kwik-Cast silicone elastomer (World Precision Instruments) until imaging.

All awake *in vivo* two-photon imaging was performed on a Leica SP8 Deep *In Vivo* Explorer (DIVE) microscope equipped with a 25× water immersion objective. On the day of testing, mice were fitted with a bespoke headplate (complete with a reservoir for holding DI water) and fixed to a headstand over a stationary running wheel. Images were acquired using LAS X software. Prior to testing, a high-resolution image was acquired to determine ROIs for each glomerulus within the field of view (2048x2048 resolution with a frame average of 2 and line average of 3, and a z stack of approximately 20um). For odor administration, a multi-channel constant-flow olfactometer[41] was placed 8 inches from the subject's nose and provided a constant stream of gentle room air from a central cannula throughout the entirety of the testing period. Mice were acclimated to the setup for at least 10 min prior to testing. A MATLAB program was developed in house to trigger image collection 10 s prior to odor administration, during 2 s odor presentation and for 8 s after odor administration. For image acquisition, resolution was decreased to 512x512 without line and frame averaging. This allowed for a sample rate of 14.65 frames per second with adequate resolution to decipher distinct glomeruli. The mice were administered a pallet of 10 distinct odors plus mineral oil in random order over the course of two separate 6-min trials. Odors included R and S limonene, isoamylacetate, 2-heptanone, acetophenone, anisole, pentanol, eugenol, butanol, and hexanone.

QUANTIFICATION AND STATISTICAL ANALYSIS

Offline analysis of *in-vitro* slice response amplitudes was performed using Clampfit 10.7.0.3 (Molecular Devices) software.

All other statistical tests were performed in GraphPad Prism version 10.0.0 for Windows, GraphPad Software, Boston, Massachusetts USA, www.graphpad.com. Differences in time to find a buried food pellet for odor detection, the number of distinct odorants each glomerulus responded to for the different genetic conditions, as well as change in external tufted cell current amplitude following stimulation of sSACs before and after application of SCH 39166 and Sulpiride were evaluated using student's t-tests. One-sample t test was used to determine if preference for a novel odor was significantly different from zero for odor discrimination. Mann-Whitney test was used to assess differences in mean frequency of mitral cells from animals with or without GABA release and with or without dopamine release due to the nonparametric distribution of the data. In all experiments, a p value less than 0.05 was considered a significant change. Statistical details including exact value of n and what n represents for each experiment are included in the text.

Supplementary Material

Refer to Web version on PubMed Central for supplementary material.

ACKNOWLEDGMENTS

Research reported in this publication was supported by the McNair Medical Institute, NIH (NINDS R01NS078294, NIDDK R01DK109934, NINDS UF1NS111692), and DOD (PR180451-PRMP) awards to B.R.A., NINDS (1K12NS098482) award to A.L.-W., as well as NIA (R21AG068607) and NIEHS (R01ES034037) to Z.F. Further support was also provided in part by the Eunice Kennedy Shriver National Institute of Child Health & Human Development of the NIH under award number P50HD103555 for use of the cell and tissue pathogenesis and viral production core facilities. The content is solely the responsibility of the authors and does not necessarily represent the official views of the NIH. The authors also wish to thank Aashka Sheth and Victor Gutierrez for assistance with behavioral experiments.

REFERENCES

1. Sámano C, Cifuentes F, and Morales MA (2012). Neurotransmitter segregation: functional and plastic implications. Prog. Neurobiol 97, 277–287. [PubMed: 22531669]
2. Svensson E, Apergis-Schoute J, Burnstock G, Nusbaum MP, Parker D, and Schiöth HB (2018). General Principles of Neuronal Co-transmission: Insights From Multiple Model Systems. Front. Neural Circ 12, 117.
3. Tritsch NX, Ding JB, and Sabatini BL (2012). Dopaminergic neurons inhibit striatal output through non-canonical release of GABA. Nature 490, 262–266. [PubMed: 23034651]
4. Tritsch NX, and Sabatini BL (2012). Dopaminergic modulation of synaptic transmission in cortex and striatum. Neuron 76, 33–50. [PubMed: 23040805]
5. Yu X, Ye Z, Houston CM, Zecharia AY, Ma Y, Zhang Z, Uygun DS, Parker S, Vyssotski AL, Yustos R, et al. (2015). Wakefulness Is Governed by GABA and Histamine Cotransmission. Neuron 87, 164–178. [PubMed: 26094607]
6. Granger AJ, Wang W, Robertson K, El-Rifai M, Zanello AF, Bistrong K, Saunders A, Chow BW, Nuñez V, Turrero García M, et al. (2020 Jul 2). Cortical ChAT+ neurons co-transmit acetylcholine and GABA in a target- and brain-region-specific manner. Elife 9, e57749. [PubMed: 32613945]
7. Vaaga CE, Borisovska M, and Westbrook GL (2014). Dual-transmitter neurons: functional implications of co-release and co-transmission. Curr. Opin. Neurobiol 29, 25–32. [PubMed: 24816154]
8. Tritsch NX, Granger AJ, and Sabatini BL (2016). Mechanisms and functions of GABA co-release. Nat. Rev. Neurosci 17, 139–145. [PubMed: 26865019]
9. Fuxe K, Dahlström AB, Jonsson G, Marcellino D, Guescini M, Dam M, Manger P, and Agnati (2010 Feb 9). The discovery of central monoamine neurons gave volume transmission to the wired brain. Prog. Neurobiol 90, 82–100. [PubMed: 19853007]
10. Maher BJ, and Westbrook GL (2008). Co-transmission of dopamine and GABA in periglomerular cells. J. Neurophysiol 99, 1559–1564. [PubMed: 18216231]
11. Hirasawa H, Betensky RA, and Raviola E (2012). Corelease of dopamine and GABA by a retinal dopaminergic neuron. J. Neurosci 32, 13281–13291. [PubMed: 22993444]
12. Zhang X, and van den Pol AN (2015). Dopamine/Tyrosine Hydroxylase Neurons of the Hypothalamic Arcuate Nucleus Release GABA, Communicate with Dopaminergic and Other Arcuate Neurons, and Respond to Dynorphin, Met-Enkephalin, and Oxytocin. J. Neurosci 35, 14966–14982. [PubMed: 26558770]
13. Kosaka T, Kosaka K, Hataguchi Y, Nagatsu I, Wu JY, Ottersen OP, Storm-Mathisen J, and Hama K (1987). Catecholaminergic neurons containing GABA-like and/or glutamic acid decarboxylase-like immunoreactivities in various brain regions of the rat. Exp. Brain Res 66, 191–210. [PubMed: 2884126]
14. Wachowiak M, and Shipley MT (2006 Aug). Coding and synaptic processing of sensory information in the glomerular layer of the olfactory bulb. Semin. Cell Dev. Biol 17, 411–423. [PubMed: 16765614]
15. Liu S, Plachez C, Shao Z, Puche A, and Shipley MT (2013). Olfactory bulb short axon cell release of GABA and dopamine produces a temporally biphasic inhibition-excitation response in external tufted cells. J. Neurosci 33, 2916–2926. [PubMed: 23407950]

16. Kiyokage E, Pan YZ, Shao Z, Kobayashi K, Szabo G, Yanagawa Y, Obata K, Okano H, Toida K, Puche AC, and Shipley MT (2010 Jan 20). Molecular identity of periglomerular and short axon cells. J. Neurosci 30, 1185–1196. [PubMed: 20089927]
17. Pinching AJ, and Powell TPS (1971). The neuron types of the glomerular layer of the olfactory bulb. J. Cell Sci 9, 305–345. [PubMed: 4108056]
18. De Saint Jan D, Hirnet D, Westbrook GL, and Charpak S (2009). External tufted cells drive the output of olfactory bulb glomeruli. J. Neurosci 29, 2043–2052. [PubMed: 19228958]
19. Liu S, Puche AC, and Shipley MT (2016). The Interglomerular Circuit Potently Inhibits Olfactory Bulb Output Neurons by Both Direct and Indirect Pathways. J. Neurosci 36, 9604–9617. [PubMed: 27629712]
20. Zhou FW, Shao ZY, Shipley MT, and Puche AC (2020). Short-term plasticity in glomerular inhibitory circuits shapes olfactory bulb output. J. Neurophysiol 123, 1120–1132. [PubMed: 31995427]
21. Shao Z, Liu S, Zhou F, Puche AC, and Shipley MT (2019). Reciprocal Inhibitory Glomerular Circuits Contribute to Excitation-Inhibition Balance in the Mouse Olfactory Bulb. eNeuro 6.
22. Murphy GJ, Darcy DP, and Isaacson JS (2005 Mar). Intraglomerular inhibition: signaling mechanisms of an olfactory microcircuit. Nat. Neurosci 8, 354–364. [PubMed: 15696160]
23. Coronas V, Srivastava LK, Liang JJ, Jourdan F, and Moyse E (1997). Identification and localization of dopamine receptor subtypes in rat olfactory mucosa and bulb: a combined in situ hybridization and ligand binding radioautographic approach. J. Chem. Neuroanat 12, 243–257. [PubMed: 9243344]
24. Koster NL, Norman AB, Richtand NM, Nickell WT, Puche AC, Pixley SK, and Shipley MT (1999). Olfactory receptor neurons express D2 dopamine receptors. J. Comp. Neurol 411, 666–673. [PubMed: 10421875]
25. Gutièrrez-Mecinas M, Crespo C, Blasco-Ibáñez JM, Gracia-Llanes FJ, Marqués-Marí AI, Nácher J, Varea E, and Martínez-Guijarro FJ (2005). Distribution of D2 dopamine receptor in the olfactory glomeruli of the rat olfactory bulb. Eur. J. Neurosci 22, 1357–1367. [PubMed: 16190891]
26. Wachowiak M, and Cohen LB (1999). Presynaptic inhibition of primary olfactory afferents mediated by different mechanisms in lobster and turtle. J. Neurosci 19, 8808–8817. [PubMed: 10516300]
27. Vaaga CE, Yorgason JT, Williams JT, and Westbrook GL (2017). Presynaptic gain control by endogenous cotransmission of dopamine and GABA in the olfactory bulb. J. Neurophysiol 117, 1163–1170. [PubMed: 28031402]
28. Liu S (2020). Dopaminergic Modulation of Glomerular Circuits in the Mouse Olfactory Bulb. Front. Cell. Neurosci 14, 172. [PubMed: 32595457]
29. Machado CF, Reis-Silva TM, Lyra CS, Felicio LF, and Malnic B (2018). Buried Food-seeking Test for the Assessment of Olfactory Detection in Mice. Bio. Protoc 8, e2897.
30. Burton SD (2017 Oct 1). Inhibitory circuits of the mammalian main olfactory bulb. J. Neurophysiol 118, 2034–2051. [PubMed: 28724776]
31. Lyons-Warren AM, Herman I, Hunt PJ, and Arenkiel BR (2021 Jun). A systematic-review of olfactory deficits in neurodevelopmental disorders: From mouse to human. Neurosci. Biobehav. Rev 125, 110–121. [PubMed: 33610612]
32. Zhou HQ, Zhuang LJ, Bao HQ, Li SJ, Dai FY, Wang P, Li Q, and Yin DM (2022). Olfactory regulation by dopamine and DRD2 receptor in the nose. Proc. Natl. Acad. Sci. USA 119, e2118570119. [PubMed: 35263227]
33. Liu G, Patel JM, Tepe B, McClard CK, Swanson J, Quast KB, and Arenkiel BR (2018). An objective and reproducible test of olfactory learning and discrimination in mice. JoVE, e57142.
34. Root DH, Zhang S, Barker DJ, Miranda-Barrientos J, Liu B, Wang HL, and Morales M (2018 Jun 19). Selective Brain Distribution and Distinctive Synaptic Architecture of Dual Glutamatergic-GABAergic Neurons. Cell Rep. 23, 3465–3479. [PubMed: 29924991]
35. Root DH, Barker DJ, Estrin DJ, Miranda-Barrientos JA, Liu B, Zhang S, Wang HL, Vautier F, Ramakrishnan C, Kim YS, et al. (2020 Sep 1). Distinct Signaling by Ventral Tegmental Area Glutamate, GABA, and Combinatorial Glutamate-GABA Neurons in Motivated Behavior. Cell Rep. 32, 108094. [PubMed: 32877676]

36. Shuen JA, Chen M, Gloss B, and Calakos N (2008). Drd1a-tdTomato BAC transgenic mice for simultaneous visualization of medium spiny neurons in the direct and indirect pathways of the basal ganglia. J. Neurosci 28, 2681–2685. [PubMed: 18337395]
37. Imamura F, Nagao H, Naritsuka H, Murata Y, Taniguchi H, and Mori K (2006). A leucine-rich repeat membrane protein, 5T4, is expressed by a subtype of granule cells with dendritic arbors in specific strata of the mouse olfactory bulb. J. Comp. Neurol 495, 754–768. [PubMed: 16506198]
38. Faedo A, Ficara F, Ghiani M, Aiuti A, Rubenstein JL, and Bulfone A (2002). Developmental expression of the T-box transcription factor T-bet/Tbx21 during mouse embryogenesis. Mech. Dev 116, 157–160. [PubMed: 12128215]
39. Nagayama S, Enerva A, Fletcher ML, Masurkar AV, Igarashi KM, Mori K, and Chen WR (2010). Differential axonal projection of mitral and tufted cells in the mouse main olfactory system. Front. Neural Circ 4, 120.
40. Spors H, Albeanu DF, Murthy VN, Rinberg D, Uchida N, Wachowiak M, and Friedrich RW (2012). Illuminating vertebrate olfactory processing. J. Neurosci 32, 14102–14108. [PubMed: 23055479]
41. Burton SD, Wipfel M, Guo M, Eiting TP, and Wachowiak M (2019 Mar 11). A Novel Olfactometer for Efficient and Flexible Odorant Delivery. Chem. Senses 44, 173–188. [PubMed: 30657873]
42. Kosaka T, Pignatelli A, and Kosaka K (2020). Heterogeneity of tyrosine hydroxylase expressing neurons in the main olfactory bulb of the mouse. Neurosci. Res 157, 15–33. Aug. [PubMed: 31629793]
43. Sethuramanujam S, McLaughlin AJ, deRosenroll G, Hoggarth A, Schwab DJ, and Awatramani GB (2016 Jun 15). A Central Role for Mixed Acetylcholine/GABA Transmission in Direction Coding in the Retina. Neuron 90, 1243–1256. [PubMed: 27238865]
44. Lee S, Kim K, and Zhou ZJ (2010 Dec 22). Role of ACh-GABA cotransmission in detecting image motion and motion direction. Neuron 68, 1159–1172. [PubMed: 21172616]
45. Banerjee A, Marbach F, Anselmi F, Koh MS, Davis MB, Garcia da Silva P, Delevich K, Oyibo HK, Gupta P, Li B, and Albeanu DF (2015 Jul 1). An Interglomerular Circuit Gates Glomerular Output and Implements Gain Control in the Mouse Olfactory Bulb. Neuron 87, 193–207. [PubMed: 26139373]
46. Tillerson JL, Caudle WM, Parent JM, Gong C, Schallert T, and Miller GW (2006 Sep 15). Olfactory discrimination deficits in mice lacking the dopamine transporter or the D2 dopamine receptor. Behav. Brain Res 172, 97–105. [PubMed: 16765459]
47. Abraham NM, Egger V, Shimshek DR, Renden R, Fukunaga I, Sprengel R, Seeburg PH, Klugmann M, Margrie TW, Schaefer AT, and Kuner T (2010 Feb 11). Synaptic inhibition in the olfactory bulb accelerates odor discrimination in mice. Neuron 65, 399–411. [PubMed: 20159452]
48. Kolling LJ, Tatti R, Lowry T, Loeven AM, Fadool JM, and Fadool DA (2022 Jul 27). Modulating the Excitability of Olfactory Output Neurons Affects Whole-Body Metabolism. J. Neurosci 42, 5966–5990. [PubMed: 35710623]
49. Roland B, Jordan R, Sosulski DL, Diodato A, Fukunaga I, Wickersham I, Franks KM, Schaefer AT, and Fleischmann A (2016 May 13). Massive normalization of olfactory bulb output in mice with a 'monoclonal nose'. Elife 5, e16335. [PubMed: 27177421]
50. Zavitz D, Youngstrom IA, Borisyuk A, and Wachowiak M (2020). Effect of Interglomerular Inhibitory Networks on Olfactory Bulb Odor Representations. J. Neurosci 40, 5954–5969. [PubMed: 32561671]
51. Bartel DL, Rela L, Hsieh L, and Greer CA (2015). Dendrodendritic synapses in the mouse olfactory bulb external plexiform layer. J. Comp. Neurol 523, 1145–1161. [PubMed: 25420934]
52. Gheusi G, Cremer H, McLean H, Chazal G, Vincent JD, and Lledo PM (2000 Feb 15). Importance of newly generated neurons in the adult olfactory bulb for odor discrimination. Proc. Natl. Acad. Sci. USA 97, 1823–1828. [PubMed: 10677540]
53. Takahashi H, Ogawa Y, Yoshihara SI, Asahina R, Kinoshita M, Kitano T, Kitsuki M, Tatsumi K, Okuda M, Tatsumi K, et al. (2016). A Subtype of Olfactory Bulb Interneurons Is Required for Odor Detection and Discrimination Behaviors. J. Neurosci 36, 8210–8227. [PubMed: 27488640]

54. Doty RL, Li C, Bagla R, Huang W, Pfeiffer C, Brosvic GM, and Risser JM (1998). SKF 38393 enhances odor detection performance. Psychopharmacology (Berl) 136, 75–82. [PubMed: 9537685]
55. Doty RL, and Risser JM (1989). Influence of the D-2 dopamine receptor agonist quinpirole on the odor detection performance of rats before and after spiperone administration. Psychopharmacology (Berl) 98, 310–315. [PubMed: 2568654]
56. Höglinger GU, Alvarez-Fischer D, Arias-Carrión O, Djufri M, Windolph A, Keber U, Borta A, Ries V, Schwarting RKW, Scheller D, and Oertel WH(2015). A new dopaminergic nigro-olfactory projection. Acta Neuropathol. 130, 333–348. [PubMed: 26072303]
57. Savitt JM, Jang SS, Mu W, Dawson VL, and Dawson TM (2005). Bcl-x is required for proper development of the mouse substantia nigra. J. Neurosci 25, 6721–6728. [PubMed: 16033881]
58. Vong L, Ye C, Yang Z, Choi B, Chua S Jr., and Lowell BB (2011 Jul 14). Leptin action on GABAergic neurons prevents obesity and reduces inhibitory tone to POMC neurons. Neuron 71, 142–154. [PubMed: 21745644]
59. Jackson CR, Ruan GX, Aseem F, Abey J, Gamble K, Stanwood G, Palmiter RD, Iuvone PM, and McMahon DG (2012). Retinal dopamine mediates multiple dimensions of light-adapted vision. J. Neurosci 32, 9359–9368. [PubMed: 22764243]
60. Tong Q, Ye CP, Jones JE, Elmquist JK, and Lowell BB (2008). Synaptic release of GABA by AgRP neurons is required for normal regulation of energy balance. Nat. Neurosci 11, 998–1000. [PubMed: 19160495]
61. Madisen L, Mao T, Koch H, Zhuo JM, Berenyi A, Fujisawa S, Hsu YW, Garcia AJ 3rd, Gu X, Zanella S, et al. (2012 Mar 25). A toolbox of Cre-dependent optogenetic transgenic mice for light-induced activation and silencing. Nat. Neurosci 15, 793–802. [PubMed: 22446880]
62. Papes F, Nakahara TS, and Camargo AP (2018). Behavioral Assays in the Study of Olfaction: A Practical Guide. Methods Mol. Biol 1820, 289–388. [PubMed: 29884953]
63. Ben-Shaul Y, and OptiMouse Y (2017). a comprehensive open source program for reliable detection and analysis of mouse body and nose positions. BMC Biol. 15, 41. [PubMed: 28506280]
64. Quast KB, Ung K, Froudarakis E, Huang L, Herman I, Addison AP, Ortiz-Guzman J, Cordiner K, Saggau P, Tolias AS, and Arenkiel BR (2017). Developmental broadening of inhibitory sensory maps. Nat. Neurosci 20, 189–199. [PubMed: 28024159]
65. Hanson E, Swanson J, and Arenkiel BR (2020 Apr 23). GABAergic Input From the Basal Forebrain Promotes the Survival of Adult-Born Neurons in the Mouse Olfactory Bulb. Front. Neural Circ 14, 17.
66. Liu G, Froudarakis E, Patel JM, Kochukov MY, Pekarek B, Hunt PJ, Patel M, Ung K, Fu CH, Jo J, et al. (2019). Target specific functions of EPL interneurons in olfactory circuits. Nat. Commun 10, 3369. [PubMed: 31358754]

Highlights

- Disruption of co-transmission in the olfactory bulb impacts olfactory function
- Both GABA and dopamine release impact odor coding by refining mitral cell firing patterns
- Co-transmission of GABA and dopamine in the olfactory bulb is spatially divergent

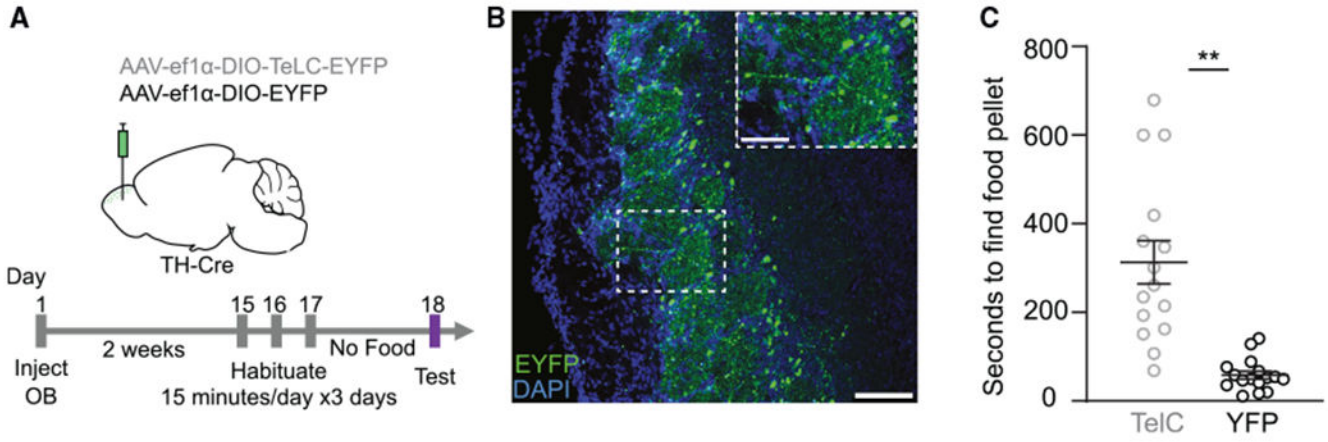

Figure 1. sSAC signaling contributes to odor detection

(A) Experimental timeline in which virus (AAV-ef1α-DIO-TeLC-EYFP or AAV-ef1α-DIO-EYFP) was injected into the bilateral olfactory bulbs (OBs) of 6-week-old *TH*-Cre mice. After 2 weeks, mice were habituated to the experimental chamber for 15 min a day for 3 days and then food restricted for 24 h prior to testing odor detection.

(B) Representative confocal image of OB glomerular layer from a mouse injected with AAV-ef1α-DIO-TeLC-EYFP showing diffuse EYFP labeling in the glomerular layer. Scale bar, 100 μm; inset scale bar, 50 μm.

(C) Results of the buried-food experiment show that mice injected with control EYFP virus (black dots) took less time to find a food pellet compared to mice injected with tetanus toxin (TeLC) virus (gray dots). Control n = 16, mean ± SEM = 58.29 ± 9.0 s; experimental n = 15, mean ± SEM = 313.1 ± 48.7 s; unpaired t test $p < 0.0001$. See also Figure S1.

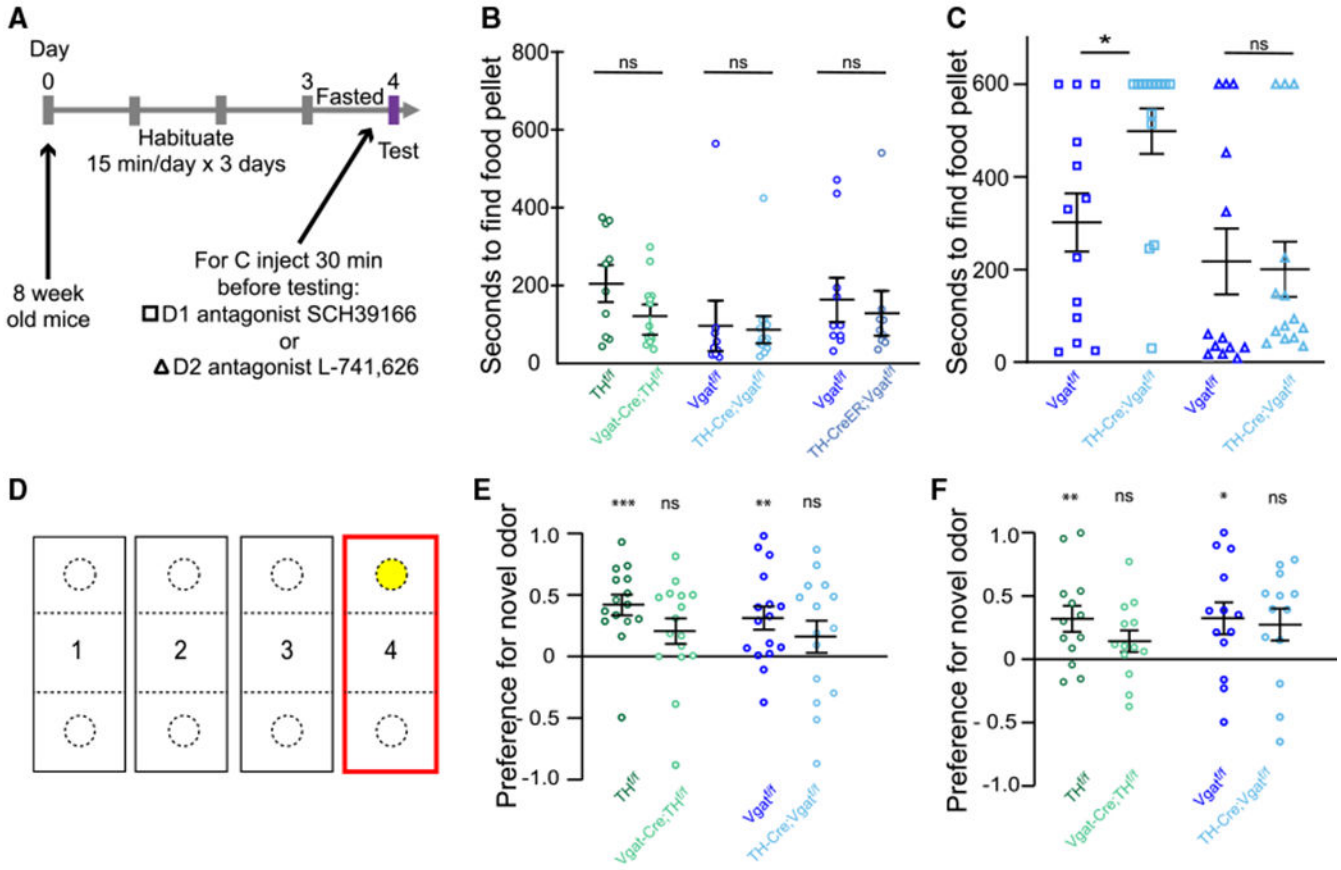

Figure 2. GABA- and D1R-mediated dopamine signaling from sSACs contribute to odor detection and discrimination

(A) Experimental timeline in which 8-week-old mice were habituated to the experimental chamber for 15 min a day for 3 days and then food restricted for 24 h.

(B) There was no difference in time to find a buried food pellet for mice lacking dopamine (light green) or GABA release (light blue) compared to littermate controls (dark green and dark blue). *TH*$^{flox/flox}$, n = 10, mean ± SEM = 209.2 ± 42.2 vs. Vgat-Cre;*TH*$^{flox/flox}$, n = 13, mean ± SEM = 125.2 ± 23.6, p = 0.08. Vgat$^{flox/flox}$, n = 9, mean ± SEM = 99.9 ± 58.9 vs. *TH*-Cre;Vgat$^{flox/flox}$, n = 13, mean ± SEM = 89.6 ± 29.2, p = 0.866. Vgat$^{flox/flox}$, n = 10, mean ± SEM = 167.9 ± 50.4 vs. *TH*-CreER;Vgat$^{flox/flox}$, n = 9, mean ± SEM = 132 ± 52.4, p = 0.628; unpaired t tests.

(C) Subcutaneous injections with a D1R antagonist (squares), but not a D2R antagonist (triangles), 30 min before testing significantly increased the amount of time for *TH*-Cre;Vgat$^{flox/flox}$ mice to find a buried food pellet compared to littermate controls receiving the same injection. *TH*-Cre;Vgat$^{flox/flox}$ + SCH39166, n = 14, mean ± SEM = 498.4 ± 49.1 vs. Vgat$^{flox/flox}$ + SCH39166, n = 13, mean ± SEM = 301.7 ± 62.8; unpaired t test $p < 0.02$. *TH*-Cre;Vgat$^{flox/flox}$ + L-741,626, n = 14, mean ± SEM = 200.1 ± 59.5 vs. Vgat$^{flox/flox}$ + L-741,626, n = 13 mean ± SEM = 217.3 ± 71.0; unpaired t test p = 0.854.

(D) Experimental design in which 8-week-old mice are placed in a chamber with two tea diffusers containing the same odor for three 2-min trials. During trial four (red box), one of the tea diffusers (yellow circle) contained a novel odor.

(E and F) Mice lacking GABA (light blue) and dopamine (light green) release from sSACs exhibited no preference for the novel odor when discriminating anisole from acetophenone (E) or isoamyl acetate from isoamylbutyrate (F). In contrast, control littermates (dark blue, dark green) exhibited a preference for the novel odor in both experiments. Acetophenone: *TH*-Cre;Vgat$^{flox/flox}$, n = 15, mean ± SEM = 0.162 ± 0.131, one-sample t test p = 0.24; Vgat-Cre;*TH*$^{flox/flox}$, n = 16, mean ± SEM = 0.207 ± 0.104, one-sample t test p = 0.07; Vgat$^{flox/flox}$, n = 16, mean ± SEM = 0.313 ± 0.095, p < 0.005; *TH*$^{flox/flox}$, n = 15, mean ± SEM = 0.419 ± 0.085, one-sample t test p < 0.001. Isoamylbuturate: n = 13 for all groups, *TH*$^{flox/flox}$, mean ± SEM = 0.320 ± 0.104, one-sample t test p < 0.01; Vgat-Cre;*TH*$^{flox/flox}$, mean ± SEM = 0.143 ± 0.086, one-sample t test p = .1212; Vgat$^{flox/flox}$, mean ± SEM = 0.325 ± 0.126 one-sample t test p < 0.05; *TH*-Cre;Vgat$^{flox/flox}$, mean ± SEM = 0.275 ± 0.126, one-sample t test p = 0.051. See also Figure S2.

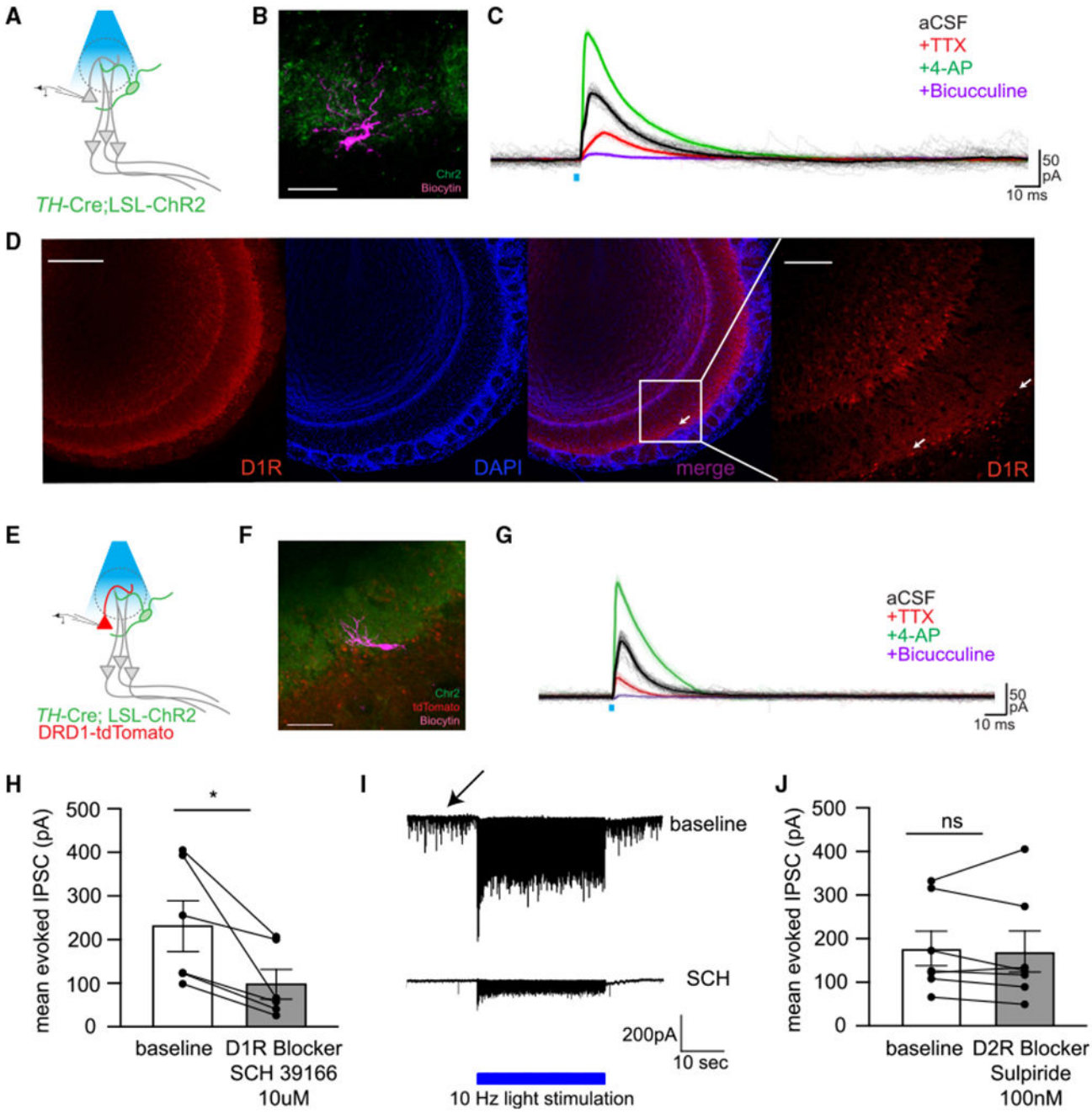

Figure 3. sSAC inhibition of ETC is modified by sSAC dopamine via D1R receptors

(A) Experimental design in which acute horizontal slices were prepared from *TH*-Cre;LSL-ChR2 mice. sSACs expressing channelrhodopsin (green cells) were stimulated with blue light while recording from external tufted cells (ETCs).

(B and C) Cell fill, scale bar 50 μm (B) and sample traces (C) from a representative ETC showing monosynaptic GABAergic connectivity.

(D) The 40-μm slices of the OB from a Drd1a-tdTomato^{tg} mouse mounted with DAPI showing red labeling throughout the OB, including the border of the glomerular layer (white arrows). Scale bar, 250 μm; inset scale bar, 100 μm.

(E) Experimental design in which acute horizontal slices were prepared from *TH*-Cre;LSL-ChR2;Drd1a-tdTomato^{tg} mice. sSACs expressing channelrhodopsin (green cells) were stimulated with blue light while recording from ETCs (red).

(F and G) Cell fill, scale bar, 50 μm (F) and sample traces (G) from a representative ETC showing monosynaptic GABAergic connectivity.

(H) Summary data showing a significant decrease in evoked inhibitory post-synaptic currents (IPSCs) following application of 10 μM D1R-specific blocker SCH39166 when stimulating sSACs expressing channelrhodopsin with blue light while recording from ETCs in horizontal slices prepared from *TH*-Cre;LSL-ChR2 mice as shown in (A). Baseline 233.3 ± 57.15 pA vs. SCH 99.6 ± 33.36 pA, paired t test p = .029, six cells across five animals, averaged across 30 s ± SEM.

(I) Sample traces from a representative ETC at baseline (top) and after application of the D1R-specific blocker SCH39166 (10 μM) (bottom) including spontaneous activity (arrow). Amplitude of spontaneous activity: baseline mean ± SEM = 47.86 ± 11.02 vs. SCH39166 11.00 ± 1.57, paired t test p = 0.012.

(J) Summary data showing no change in evoked IPSCs following application of 100 nM sulpiride, a D2R-specific blocker. Baseline 177.7 ± 39.68 pA vs. sulpiride 170.8 ± 47.09 pA, paired t test p = 0.66, seven cells across six animals, averaged across 30 s ± SEM. See also Figure S3.

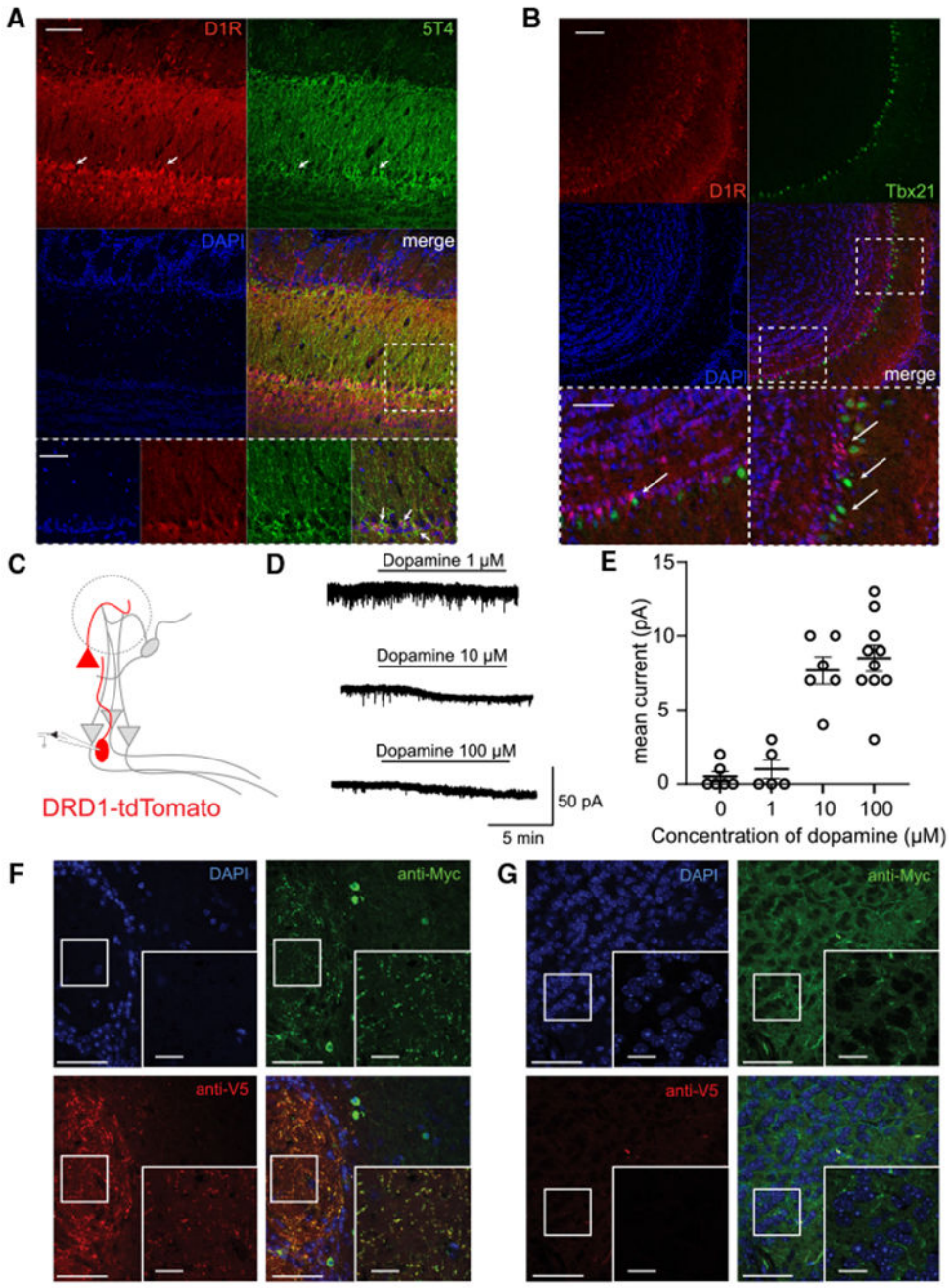

Figure 4. Granule cells receive dopaminergic input from sSACs

(A and B) Horizontal OB slices from a Drd1a-tdTomato^{tg} mouse mounted with DAPI (A) stained with a subtype-specific marker for granule cells, anti-5T4, primary antibody followed by Alexa 488 secondary antibody showing colocalization (arrows), suggesting granule cells express D1R, and (B) stained with a mitral cell marker, anti-Tbx21, primary antibody followed by Alexa 488 secondary antibody without colocalization (arrows). Scale bars, 100 μm; inset scale bars, 50 μm.

(C) Experimental design in which acute horizontal slices were prepared from Drd1a-tdTomato^{tg} mice to record from red-labeled granule cells.
(D) Representative voltage-clamp recordings from tdTomato-expressing granule cells show depolarizing currents in response to 1 (top), 10 (middle), and 100 (bottom) μM dopamine application.
(E) Summary data showing mean ± SEM current amplitude for saline, as well as increasing concentrations of dopamine. Data collected from 11 animals total.
(F and G) The 25 μM horizontal OB slice mounted with DAPI from a *TH*-Cre mouse injected with AAV-ef1α-DIO-VMAT2-myc and AAV-ef1α-DIO-VGAT-V5 stained with anti-myc and anti-V5 primary antibodies followed by Alexa 488 and 564 secondary antibodies showing diffuse expression of both markers in the glomerular cell layer (F) but only anti-myc in the granule cell layer (G) at low and high magnification (insets), suggesting GABAergic and dopaminergic signaling from sSACs in the glomerular layer but only dopaminergic signaling in the granule cell layer. All scale bars, 45 μm. See also Figures S4 and S5.

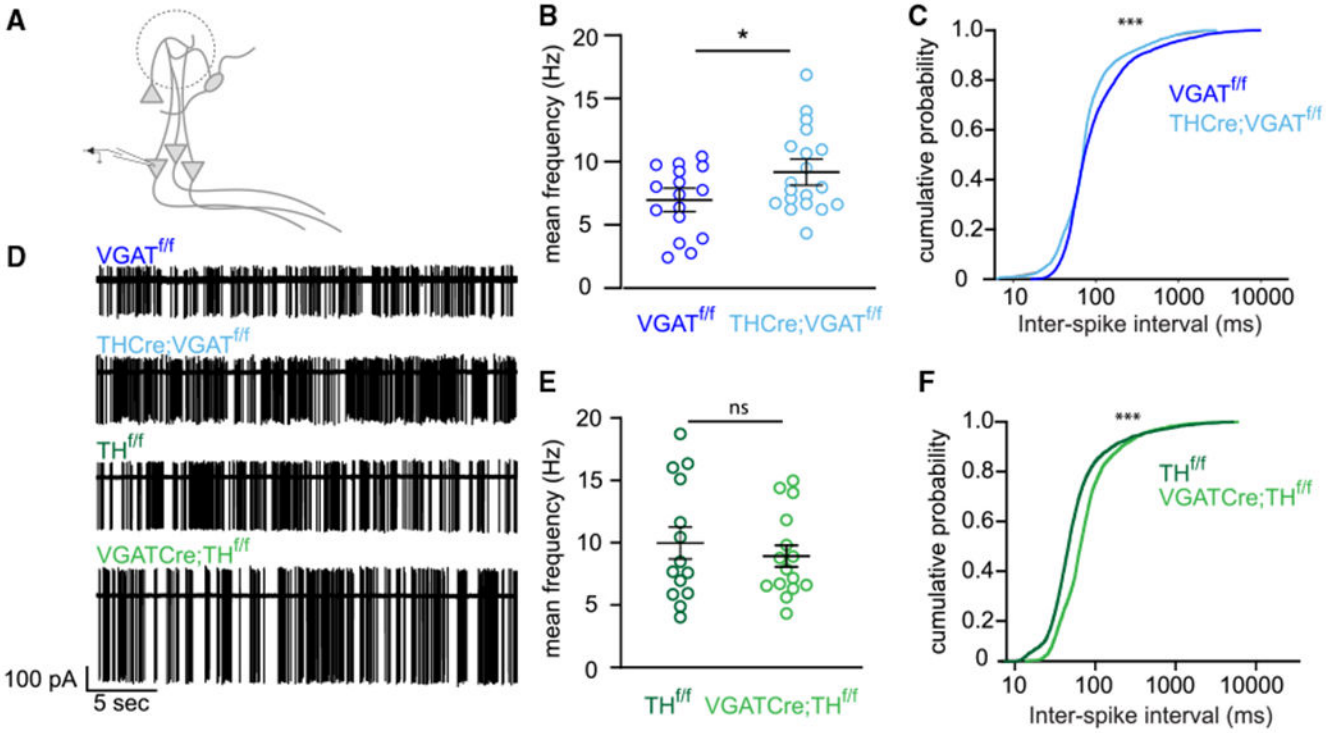

Figure 5. Loss of sSAC GABA increases spontaneous mitral cell firing

(A) Experimental design in which acute horizontal slices were prepared and spontaneous firing rates measured from mitral cells identified based on shape and location.

(B and C) *TH*-Cre;Vgat$^{flox/flox}$ mice exhibited an increased mean firing frequency (light blue dots, n = 6 mice, n = 19 cells, mean ± SEM firing rate 9.18 ± 0.75 Hz) compared to littermate controls (dark blue dots, n = 6 mice, n = 16 cells, mean ± SEM firing rate 6.98 ± 0.67 Hz); unpaired t test, p = 0.04 (B) and a reduced interspike interval (C) Kolmogorov-Smirnov test, D = 0.0908, p < 0.0001.

(D) Representative traces of all four conditions.

(E and F) Vgat-Cre; *TH*$^{flox/flox}$ mice (light green dots, n = 5 mice, n = 15 cells, mean ± SEM firing rate 8.925 ± 0.874 Hz) did not exhibit any change in mean firing frequency compared to littermate controls (dark green dots, n = 5 mice, n = 14 cells, mean ± SEM firing rate 9.977 ± 1.284 Hz); unpaired t test, p = 0.499 (E), but interspike interval (F) was significantly different; Kolmogorov-Smirnov test. D = 0.2621, p < 0.0001.

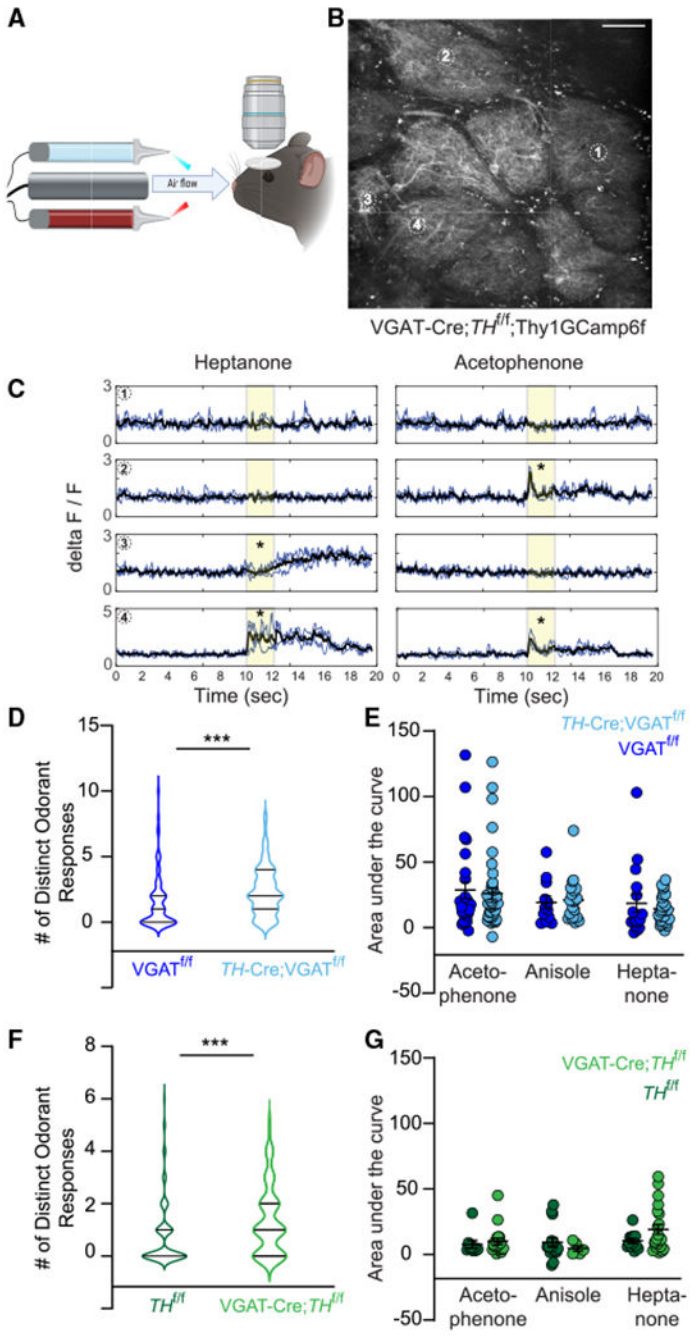

Figure 6. Loss of GABA or dopamine increases glomerular responses to odor

(A) Experimental design in which glomeruli were imaged through a cranial window over the OB while presenting odors.

(B) Representative high-resolution image of glomeruli from a Vgat-Cre; *TH*$^{flox/flox}$;Thy1Gcamp6f mouse showing 11 glomeruli, of which four have been numbered (circles). Scale bar, 50 μm.

(C) Example traces of change in fluorescence from the four glomeruli labeled in (B) in response to heptanone and acetophenone (yellow bar indicates duration of odor presentation)

illustrating the variation in response patterns with some glomeruli not responding (asterisk) to either odor (#1), one odor (#2, 3), or both odors (#4) with variable temporal patterns.
(D) Violin plots showing the distribution of the number of unique odors a given glomerulus responded to for mice lacking GABA release from sSACs (light blue, n = 10 mice, N = 107 glomeruli, mean ± SEM = 2.336 ± 0.179 odors, median = 2) compared to littermate controls (dark blue, n = 8 mice, N = 87 glomeruli, mean ± SEM = 1.494 ± 0.217 odors, median = 1); Mann-Whitney U test, $p < 0.0001$. (E) Magnitude of mitral cell response quantified as area under the curve for glomeruli that responded to acetophenone, anisole, and heptanone with no differences observed between control (dark blue dots) or experimental (light blue dots) animals. Response to acetophenone: *TH*-Cre;Vgat$^{flox/flox}$;Thy1GCamp6f, n = 43, mean = 26.09 ± 4.28; Vgat$^{flox/flox}$;Thy1GCamp6f, n = 26, mean = 28.69 ± 6.43; unpaired t test p = 0.7278. Response to anisole: *TH*-Cre;Vgat$^{flox/flox}$;Thy1GCamp6f, n = 20, mean = 21.14 ± 3.61; VGAT$^{flox/flox}$;Thy1GCamp6f, n = 12, mean = 19.21 ± 4.79; unpaired t test p = 0.7483. Response to heptanone, *TH*-Cre;Vgat$^{flox/flox}$;Thy1GCamp6f, n = 29, mean = 14.47 ± 1.95; VGAT$^{flox/flox}$;Thy1GCamp6f, n = 16, mean = 18.65 ± 6.98; unpaired t test p = 0.4726.
(F) Violin plot showing distribution of number of unique odors a given glomerulus responded to for mice lacking dopamine release from sSACs (light green, n = 8 mice, N = 84 glomeruli, mean ± SEM = 1.32 ± 0.140 odors, median = 1) compared to littermate controls (dark green, n = 10 mice, N = 105 glomeruli, mean ± SEM = 0.79 ± 0.124 odors, median = 0); Mann-Whitney U test p = 0.0003.
(G) Magnitude of mitral cell response quantified as area under the curve for glomeruli that responded to acetophenone, anisole, and heptanone with no difference between control (dark green dots) or experimental (light green dots) animals. Response to acetophenone: Vgat-Cre;*TH*$^{flox/flox}$;Thy1GCamp6f, n = 19, mean = 10.04 ± 2.37; *TH*$^{flox/flox}$;Thy1GCamp6f, n = 9, mean = 7.76 ± 3.05; unpaired t test p = 0.5779. Response to anisole: Vgat-Cre;*TH*$^{flox/flox}$;Thy1GCamp6f, n = 5, mean = 4.74 ± 2.07; *TH*$^{flox/flox}$;Thy1GCamp6f, n = 15, mean = 9.296 ± 3.53; unpaired t test p = 0.4811. Response to heptanone: Vgat-Cre;*TH*$^{flox/flox}$;Thy1GCamp6f, n = 21, mean = 19.16 ± 3.80; *TH*$^{flox/flox}$;Thy1GCamp6f, n = 12, mean = 10.34 ± 1.84; unpaired t test p = 0.41051.

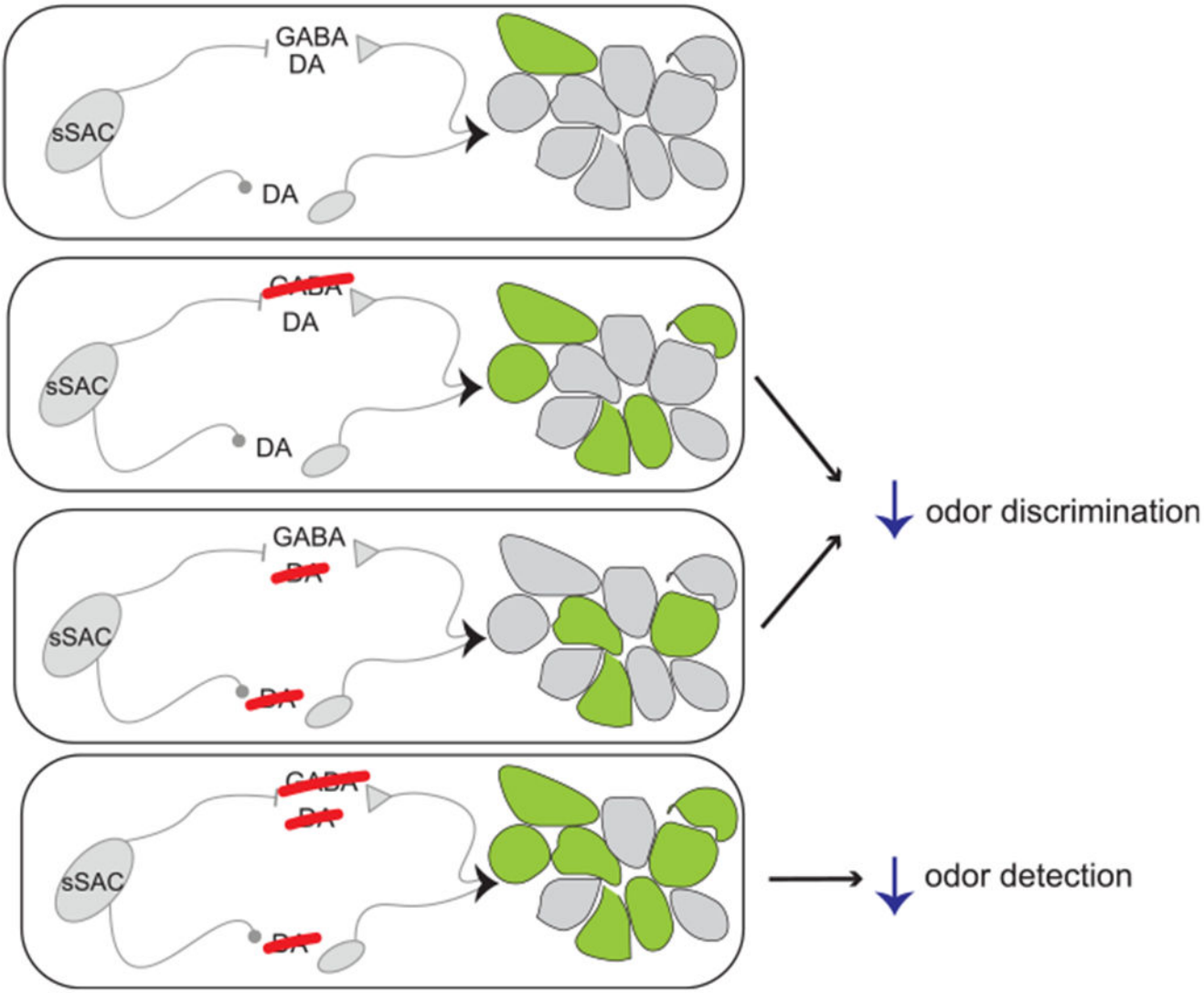

Figure 7. Model of proposed connectivity for co-transmission

Under typical conditions, odor-evoked activity in mitral cells results in sparse glomerular patterning due to GABAergic and dopaminergic signaling from sSACs (top). Loss of GABA or dopamine (middle) increases the number of glomeruli that respond to any given odor and impairs odor discrimination but not odor detection. Loss of both GABA and dopamine (bottom) impairs odor detection, which is proposed to be due to even higher increases in mitral cell signaling.

KEY RESOURCES TABLE

REAGENT or RESOURCE	SOURCE	IDENTIFIER
Antibodies		
Rabbi anti-TH antibody	Chemicon	Cat# AB152, 1:1000
Chicken anti-GFP antibody	Abcam	Cat# AB13970, 1:1000
Rabbit anti-CCK antibody	Sigma Aldrich	Cat# C2581, 1:1000
Sheep anti-5T4 antibody	R&D systems	Cat# AF5049, 1:1000
mouse anti-myc antibody	Thermofisher	Cat# 13–2500, 1:200
Rat anti-V5 antibody	Ab-cam	Cat# AB206571; 1:1000
Rabbit anti-Tbx21	Gift from Mitsui Lab	1:500
Bacterial and virus strains		
AAV-ef1a-DIO-TeLC-EYFP	Arenkiel Lab	
AAV-ef1a-DIO-EYFP	gift from Karl Deisseroth	RRID:Addgene_27056
AAV-EF1a-DIO-VMAT2-myc	(Tritsch et al.)[3]	RRID:Addgene_39339
AAV-EF1a-DIO-VGAT-V5	Arenkiel Lab	
AAV-ef1a-FlpDIO-Cre	Arenkiel Lab	
Chemicals, peptides, and recombinant proteins		
SCH39166	Tocris	Cat# 2299
L-741,626	Tocris	Cat# 1003
Sulpiride	Tocris	Cat# 0895
DMSO	Tocris	Cat #3176
Dopamine	Tocris	Cat #1534
isoamylacetate	Sigma Aldrich	Cat# W205508
isoamylbuturate	Sigma Aldrich	Cat# W206008
Pentanol	Sigma Aldrich	Cat# 138975
Hexanol	Sigma Aldrich	Cat# H-13303
S+ Carvone	Sigma Aldrich	Cat# 22070
S− Carvone	Sigma Aldrich	Cat# 124931
Experimental models: Organisms/strains		
B6.Cg-*7630403G23Rik*$^{Tg(Th-cre)1Tmd}$/J	Jax laboratories (Savitt et al., 2005)[57]	Cat# 008601; RRID:IMSR_JAX:008601
B6J.129S6(FVB)-*Slc32a1*$^{tm2(cre)Lowl}$/MwarJ	Jax laboratories (Vong et al., 2011)[58]	Cat# 028862; RRID:IMSR_JAX:028862
TH$^{flox/flox}$ mice	gift of Martin Darvas	(Jackson et al., 2012)[59]
Slc32a1^{tm1Lowl}/J	Jax laboratories (Tong et al., 2008)[60]	Cat# 012897; RRID:IMSR_JAX:012897
B6; 129-*Th*$^{tm1(cre/Esr1)Nat}$/J	Jax laboratories	Cat# 008532; RRID:IMSR_JAX:008532
B6.Cg-*Slc32a1*$^{tm1.1(flpo)Hze}$/J	Jax laboratories	Cat# 029591 RRID:IMSR_JAX:029591
B6.Cg-*Gt(ROSA)26Sor*$^{tm32(CAG-COP4*H134R/EYFP)Hze}$/J (commonly known as Ai32)	Jax laboratories (Madisen et al., 2012)[61]	Cat# 024109; RRID:IMSR_JAX:02410
B6.Cg-Tg(Drd1a-tdTomato)6Calak/J	Jax laboratories (Shuen et al., 2008)[36]	Cat# 016204; RRID:IMSR_JAX:016204
C57BL/6J-Tg(Thy1-GCaMP6f)GP5.17Dkim/J	Jax laboratories	Cat# 025393; RRID:IMSR_JAX:025393

REAGENT or RESOURCE	SOURCE	IDENTIFIER
Software and algorithms		
MATLAB version v9.12 (R2022a)	Mathworks	*RRID*:SCR_001622
GraphPad Prism version 10.0.3 (217)	www.graphpad.com	*RRID*:SCR_002798